

# Associated Production of Neutral Higgs Boson with Squark Pair in the Minimal Supersymmetric Standard Model with Explicit CP Violation at the LHC

Zhao Li,<sup>\*</sup> Chong Sheng Li,<sup>†</sup> and Qiang Li<sup>‡</sup>

*Department of Physics, Peking University, 100871, Beijing*

PACS numbers: 12.60.Jv, 14.80.Cp, 14.80.Ly

## Abstract

We investigate the associated production of a neutral Higgs boson with squark pair in the minimal supersymmetric standard model without and with explicit CP violation, respectively. We discuss the constraints on the relevant parameters of the explicit CP violation by electric dipole moment experiments. Using the allowed ranges of the parameters, we show that the dominant productions in both cases are always ones of a lightest neutral Higgs boson associated with lightest stop pair, which can reach a few pb. In most of the parameter space, the total cross sections in the case with explicit CP violation are significantly enhanced, compared with ones in the case without explicit CP violation. For some special parameters, the enhancements of a few order of magnitudes can be obtained.

---

<sup>\*</sup>Electronic address: zhli.phy@pku.edu.cn

<sup>†</sup>Electronic address: csli@pku.edu.cn

<sup>‡</sup>Electronic address: qliphy@pku.edu.cn

## I. INTRODUCTION

The parameters in the Lagrangian of the minimal supersymmetric standard model (MSSM) are generally real, but it is not necessary. In general, there is not any reason that requires the parameters to be real, and the complex parameters probably can generate some new phenomenology for the CP violation. For example, after introducing the complex parameters in the mass matrices of the third generation squarks, the explicit CP violation (CPV) can be induced in the Higgs sector through the loop corrections in the Higgs effective potential[1, 2].

The MSSM with the CP conservation (CPC) provides three neutral Higgs bosons: one CP odd boson ( $A^0$ ) and two CP even boson ( $h^0, H^0$ ), whose mass eigenstates are also their CP eigenstates. However, in the MSSM with the explicit CP violation, the CP violation can introduce the mixing of the three neutral Higgs bosons, and the CP eigenstates no longer exist. Those mixing can form three new mass eigenstates of the neutral Higgs bosons:  $h_1$ ,  $h_2$  and  $h_3$ , and the all couplings involved the neutral Higgs bosons are changed[1, 2].

The previous studies have shown that the explicit CP violation mentioned above can significantly change the predictions for the Higgs productions and decays [1, 2, 3, 4]. Especially, Q. H. Cao et al.[4] recently found that there is a parameter region, in which the Higgs production cross sections via gluon fusion can be greatly enhanced with large CP phase angle. In their calculations they did not consider the constraints on the parameters from the experiments of the electric dipole moments(EDMs), because they believe that there are possible cancellations between different contributions to the electric dipole moments.

However, actually, the present experiments of the electric dipole moments[5, 6, 7, 8] have put some constraints on the parameter space in the MSSM with the explicit CP violation in some scenario. Therefore, it is necessary to make further investigation on the productions of the Higgs bosons with large CP phase angle, using the EDMs constraints on the relevant parameters. Also, B-physics and K-physics may provide the constraints on the parameters, but they depend strongly on the flavor structure in supersymmetry breaking[4], and the constraints potentially arising from B-physics and K-physics are not considered in this paper.

In this paper, we first consider the experiment constraints on the relevant parameters of the CP violation from the EDMs, and then within the allowed parameter spaces, we investigate the Higgs productions associated with the squark pairs in the MSSM with the

explicit CP violation at the CERN Large Hardron Collider (LHC) [9, 10, 11, 12, 13, 14]:

$$p + p \rightarrow \tilde{q} + \tilde{q}'^* + \Phi, \quad (1)$$

where  $\Phi$  represents the neutral Higgs bosons, although a similar process, the productions of the Higgs associated with the squark pairs, has been calculated in the minimal supergravity (mSUGRA) without the CP violation in Ref.[15].

The paper is organized as follows. In Section II we review the explicit CP violation in the MSSM. In Section III we briefly review the present theoretical analysis on the electron dipole moments of the electron and the atoms. In Section IV we show the detailed calculation of the Higgs productions associated with the squark pairs. In Section V we present the numerical results and the discussions.

## II. NEUTRAL HIGGS SECTOR IN THE MSSM WITH EXPLICIT CP VIOLATION

In order to make our paper self-contained, we briefly review the neutral Higgs sector in the MSSM with the explicit CP violation, as shown in Ref.[2].

The MSSM has two Higgs doublets  $H_1$  and  $H_2$ , whose neutral components can be written as

$$H_1^0 = \frac{1}{\sqrt{2}}(\phi_1 + ia_1); \quad H_2^0 = \frac{e^{i\xi}}{\sqrt{2}}(\phi_2 + ia_2), \quad (2)$$

where  $\phi_{1,2}$  and  $a_{1,2}$  are real fields. Their vacuum expectation values (VEV) are  $\langle \phi_{1,2} \rangle = v_{1,2}$  and  $\langle a_{1,2} \rangle = 0$ .

The one-loop effective potential of the neutral Higgs sector[16] is given by

$$V_{\text{Higgs}} = \frac{1}{2}m_1^2(\phi_1^2 + a_1^2) + \frac{1}{2}m_2^2(\phi_2^2 + a_2^2) - |m_{12}^2|(\phi_1\phi_2 - a_1a_2)\cos(\xi + \theta_{12}) \\ - |m_{12}^2|(\phi_1a_2 + \phi_2a_1)\sin(\xi + \theta_{12}) + \frac{\hat{g}^2}{8}\mathcal{D}^2 + \frac{1}{64\pi^2}\text{Str} \left[ \mathcal{M}^4 \left( \log \frac{\mathcal{M}^2}{Q_0^2} - \frac{3}{2} \right) \right], \quad (3)$$

where  $m_1$ ,  $m_2$  and  $m_{12}^2$  are the soft breaking parameters at the renormalization scale  $Q_0$ , and  $m_{12}^2 = |m_{12}^2|e^{i\theta_{12}}$  can be complex.  $\mathcal{M}$  is the field-dependent mass matrix of all modes that couple to the Higgs bosons, including the contributions of vector bosons, Higgs bosons, and fermions as well as their supersymmetric partners. Among these contributions, the dominant ones come from the third generation quarks and squarks[17].  $\mathcal{D}$  and  $\hat{g}^2$  are defined as

$$\mathcal{D} = \phi_2^2 + a_2^2 - \phi_1^2 - a_1^2 \quad (4)$$

and

$$\hat{g}^2 = \frac{g_1^2 + g_2^2}{4}, \quad (5)$$

respectively, where  $g_1$  and  $g_2$  represent the  $U(1)_Y$  and  $SU(2)_L$  gauge couplings, respectively.

The masses of the third generation quarks are

$$m_b^2 = \frac{1}{2}|h_b|^2 (\phi_1^2 + a_1^2), \quad m_t^2 = \frac{1}{2}|h_t|^2 (\phi_2^2 + a_2^2), \quad (6)$$

where  $h_b$  and  $h_t$  are the Yukawa couplings, which are given by

$$h_b = \frac{g_2 m_b}{\sqrt{2} m_W \cos \beta}, \quad h_t = \frac{g_2 m_t}{\sqrt{2} m_W \sin \beta}. \quad (7)$$

In order to calculate the Higgs masses from the effective potential (3), we need to introduce the squark mass matrices:

$$\mathcal{M}_t^2 = \begin{pmatrix} m_Q^2 + m_t^2 - \frac{1}{8} \left( g_2^2 - \frac{g_1^2}{3} \right) \mathcal{D} & -h_t^* [A_t^* (H_2^0)^* + \mu H_1^0] \\ -h_t [A_t H_2^0 + \mu^* (H_1^0)^*] & m_U^2 + m_t^2 - \frac{g_1^2}{6} \mathcal{D} \end{pmatrix}, \quad (8)$$

$$\mathcal{M}_b^2 = \begin{pmatrix} m_Q^2 + m_b^2 + \frac{1}{8} \left( g_2^2 + \frac{g_1^2}{3} \right) \mathcal{D} & -h_b^* [A_b^* (H_1^0)^* + \mu H_2^0] \\ -h_b [A_b H_1^0 + \mu^* (H_2^0)^*] & m_D^2 + m_b^2 + \frac{g_1^2}{12} \mathcal{D} \end{pmatrix}.$$

In Eq.(8),  $m_Q^2$ ,  $m_U^2$  and  $m_D^2$  are the real soft breaking parameters,  $A_b$  and  $A_t$  are the complex soft breaking parameters, and  $\mu$  is the Higgsino mass parameter. The squark mass matrices can be diagonalized by the unitary matrices  $\mathcal{R}^{\tilde{q}}$ :

$$\mathcal{R}^{\tilde{q}} = \begin{pmatrix} 1 & 0 \\ 0 & e^{i\delta_q} \end{pmatrix} \begin{pmatrix} \cos \theta_q & \sin \theta_q \\ -\sin \theta_q & \cos \theta_q \end{pmatrix}, \quad \mathcal{R}^{\tilde{q}} \mathcal{M}_q^2 (\mathcal{R}^{\tilde{q}})^\dagger = \begin{pmatrix} m_{q_1}^2 & 0 \\ 0 & m_{q_2}^2 \end{pmatrix}. \quad (9)$$

Then we can obtain the mass eigenvalues as follows:

$$\begin{aligned} m_{\tilde{t}_{1,2}}^2 &= \frac{1}{2} \left[ m_Q^2 + m_U^2 + |h_t|^2 (\phi_2^2 + a_2^2) - \frac{\hat{g}}{2} \mathcal{D} \right. \\ &\quad \left. \mp \left\{ \left( m_Q^2 - m_U^2 - \frac{3g_2^2 - 5g_1^2}{24} \mathcal{D} \right)^2 + 2|h_t|^2 |A_t e^{i\xi} (\phi_2 + ia_2) + \mu^* (\phi_1 - ia_1)|^2 \right\}^{1/2} \right]; \\ m_{\tilde{b}_{1,2}}^2 &= \frac{1}{2} \left[ m_Q^2 + m_D^2 + |h_b|^2 (\phi_1^2 + a_1^2) + \frac{\hat{g}}{2} \mathcal{D} \right. \\ &\quad \left. \mp \left\{ \left( m_Q^2 - m_D^2 + \frac{3g_2^2 - g_1^2}{24} \mathcal{D} \right)^2 + 2|h_b|^2 |A_b (\phi_1 + ia_1) + \mu^* e^{-i\xi} (\phi_2 - ia_2)|^2 \right\}^{1/2} \right]. \end{aligned} \quad (10)$$

Substituting the eigenvalues (6) and (10) into the potential (3), we get the explicit expression with the contributions of the third generation quarks and squarks, which include

the overall factors -4 for quarks and +2 for squarks. Computing the second derivatives of the potential (3) at its minimum, we will get the Higgs mass matrix for  $a_1$ ,  $a_2$ ,  $\phi_1$  and  $\phi_2$ . We can find the state  $G^0 = a_1 \cos \beta - a_2 \sin \beta$ , where  $\tan \beta = v_2/v_1$ , describes the massless Goldstone mode, which is "eaten" by the longitudinal Z boson. Then we have only three states  $a = a_1 \sin \beta + a_2 \cos \beta$ ,  $\phi_1$  and  $\phi_2$  for the squared mass matrix  $\mathcal{M}_H^2$ , which is real and symmetric. The explicit expressions of its elements are presented below[2].

The a-a element of the squared mass matrix is

$$\mathcal{M}_H^2|_{aa} = m_A^2 + \frac{3}{8\pi^2} \left\{ \frac{|h_t|^2 m_t^2}{\sin^2 \beta} g(m_{\tilde{t}_1}^2, m_{\tilde{t}_2}^2) \Delta_{\tilde{t}}^2 + \frac{|h_b|^2 m_b^2}{\cos^2 \beta} g(m_{\tilde{b}_1}^2, m_{\tilde{b}_2}^2) \Delta_{\tilde{b}}^2 \right\}, \quad (11)$$

where

$$\Delta_{\tilde{t}} = \frac{Im(A_t \mu e^{i\xi})}{m_{\tilde{t}_2}^2 - m_{\tilde{t}_1}^2}, \quad \Delta_{\tilde{b}} = \frac{Im(A_b \mu e^{i\xi})}{m_{\tilde{b}_2}^2 - m_{\tilde{b}_1}^2}, \quad g(m_1^2, m_2^2) = 2 - \frac{m_1^2 + m_2^2}{m_1^2 - m_2^2} \log \frac{m_1^2}{m_2^2}, \quad (12)$$

and

$$m_A^2 = \frac{2m_{12}^2 \cos(\xi + \theta_{12})}{\sin(2\beta)} + \frac{2}{\sin(2\beta)} \left\{ |h_t|^2 Re(A_t \mu e^{i\xi}) F(m_{\tilde{t}_1}^2, m_{\tilde{t}_2}^2) + |h_b|^2 Re(A_b \mu e^{i\xi}) F(m_{\tilde{b}_1}^2, m_{\tilde{b}_2}^2) \right\}, \quad (13)$$

with

$$F(m_a^2, m_b^2) = \frac{3(f(m_a^2) - f(m_b^2))}{32\pi^2(m_b^2 - m_a^2)}, \quad f(m^2) = 2m^2 \left( \log \frac{m^2}{Q_0^2} - 1 \right). \quad (14)$$

The  $a - \phi_1$  and  $a - \phi_2$  elements are

$$\begin{aligned} \mathcal{M}_H^2|_{a\phi_1} &= \frac{3}{16\pi^2} \left\{ \frac{m_t^2 \Delta_{\tilde{t}}}{\sin \beta} \left[ g(m_{\tilde{t}_1}^2, m_{\tilde{t}_2}^2) (X_t \cot \beta - 2|h_t|^2 R_t) - \hat{g}^2 \cot \beta \log \frac{m_{\tilde{t}_2}^2}{m_{\tilde{t}_1}^2} \right] \right. \\ &\quad \left. + \frac{m_b^2 \Delta_{\tilde{b}}}{\cos \beta} \left[ -g(m_{\tilde{b}_1}^2, m_{\tilde{b}_2}^2) (X_b + 2|h_b|^2 R'_b) + (\hat{g}^2 - 2|h_b|^2) \log \frac{m_{\tilde{b}_2}^2}{m_{\tilde{b}_1}^2} \right] \right\}, \\ \mathcal{M}_H^2|_{a\phi_2} &= \frac{3}{16\pi^2} \left\{ \frac{m_t^2 \Delta_{\tilde{t}}}{\sin \beta} \left[ -g(m_{\tilde{t}_1}^2, m_{\tilde{t}_2}^2) (X_t + 2|h_t|^2 R'_t) + (\hat{g}^2 - 2|h_t|^2) \log \frac{m_{\tilde{t}_2}^2}{m_{\tilde{t}_1}^2} \right] \right. \\ &\quad \left. + \frac{m_b^2 \Delta_{\tilde{b}}}{\cos \beta} \left[ g(m_{\tilde{b}_1}^2, m_{\tilde{b}_2}^2) (X_b \tan \beta - 2|h_b|^2 R_b) - \hat{g}^2 \tan \beta \log \frac{m_{\tilde{b}_2}^2}{m_{\tilde{b}_1}^2} \right] \right\}, \end{aligned}$$

where

$$\begin{aligned} X_t &= \frac{(5g_1^2 - 3g_2^2)(m_Q^2 - m_U^2)}{12(m_{\tilde{t}_2}^2 - m_{\tilde{t}_1}^2)}, & X_b &= \frac{(g_1^2 - 3g_2^2)(m_Q^2 - m_D^2)}{12(m_{\tilde{b}_2}^2 - m_{\tilde{b}_1}^2)}, \\ R_t &= \frac{|\mu|^2 \cot \beta + Re(A_t \mu e^{i\xi})}{m_{\tilde{t}_2}^2 - m_{\tilde{t}_1}^2}, & R'_t &= \frac{|A_t|^2 + Re(A_t \mu e^{i\xi}) \cot \beta}{m_{\tilde{t}_2}^2 - m_{\tilde{t}_1}^2}, \\ R_b &= \frac{|\mu|^2 \tan \beta + Re(A_b \mu e^{i\xi})}{m_{\tilde{b}_2}^2 - m_{\tilde{b}_1}^2}, & R'_b &= \frac{|A_b|^2 + Re(A_b \mu e^{i\xi}) \tan \beta}{m_{\tilde{b}_2}^2 - m_{\tilde{b}_1}^2}. \end{aligned} \quad (15)$$

The other elements of the squared mass matrix are

$$\begin{aligned} \mathcal{M}_H^2|_{\phi_1\phi_1} &= M_Z^2 \cos^2 \beta + m_A^2 \sin^2 \beta \\ &+ \frac{3m_t^2}{8\pi^2} \left[ g(m_{\tilde{t}_1}^2, m_{\tilde{t}_2}^2) R_t (|h_t|^2 R_t - \cot\beta X_t) + \hat{g}^2 \cot\beta R_t \log \frac{m_{\tilde{t}_2}^2}{m_{\tilde{t}_1}^2} \right] \\ &+ \frac{3m_b^2}{8\pi^2} \left\{ |h_b|^2 \log \frac{m_{\tilde{b}_1}^2 m_{\tilde{b}_2}^2}{m_b^4} - \hat{g}^2 \log \frac{m_{\tilde{b}_1}^2 m_{\tilde{b}_2}^2}{Q_0^4} \right. \\ &\quad \left. + g(m_{\tilde{b}_1}^2, m_{\tilde{b}_2}^2) R'_b (|h_b|^2 R'_b + X_b) + \log \frac{m_{\tilde{b}_2}^2}{m_{\tilde{b}_1}^2} [X_b + (2|h_b|^2 - \hat{g}^2) R'_b] \right\}, \end{aligned}$$

$$\begin{aligned} \mathcal{M}_H^2|_{\phi_1\phi_2} &= - (M_Z^2 + m_A^2) \sin \beta \cos \beta \\ &+ \frac{3m_t^2}{8\pi^2} \left\{ g(m_{\tilde{t}_1}^2, m_{\tilde{t}_2}^2) \left[ |h_t|^2 R_t R'_t + \frac{X_t}{2} (R_t - R'_t \cot\beta) \right] + \frac{\hat{g}^2}{2} \cot\beta \log \frac{m_{\tilde{t}_1}^2 m_{\tilde{t}_2}^2}{Q_0^4} \right. \\ &\quad \left. + \log \frac{m_{\tilde{t}_2}^2}{m_{\tilde{t}_1}^2} \left[ |h_t|^2 R_t - \frac{X_t}{2} \cot\beta + \frac{\hat{g}^2}{2} (R'_t \cot\beta - R_t) \right] \right\} \\ &+ \frac{3m_b^2}{8\pi^2} \left\{ g(m_{\tilde{b}_1}^2, m_{\tilde{b}_2}^2) \left[ |h_b|^2 R_b R'_b + \frac{X_b}{2} (R_b - R'_b \tan\beta) \right] + \frac{\hat{g}^2}{2} \tan\beta \log \frac{m_{\tilde{b}_1}^2 m_{\tilde{b}_2}^2}{Q_0^4} \right. \\ &\quad \left. + \log \frac{m_{\tilde{b}_2}^2}{m_{\tilde{b}_1}^2} \left[ |h_b|^2 R_b - \frac{X_b}{2} \tan\beta + \frac{\hat{g}^2}{2} (R'_b \tan\beta - R_b) \right] \right\}, \end{aligned}$$

$$\begin{aligned} \mathcal{M}_H^2|_{\phi_2\phi_2} &= M_Z^2 \sin^2 \beta + m_A^2 \cos^2 \beta \\ &+ \frac{3m_t^2}{8\pi^2} \left\{ |h_t|^2 \log \frac{m_{\tilde{t}_1}^2 m_{\tilde{t}_2}^2}{m_t^4} - \hat{g}^2 \log \frac{m_{\tilde{t}_1}^2 m_{\tilde{t}_2}^2}{Q_0^4} \right. \\ &\quad \left. + g(m_{\tilde{t}_1}^2, m_{\tilde{t}_2}^2) R'_t (|h_t|^2 R'_t + X_t) + \log \frac{m_{\tilde{t}_2}^2}{m_{\tilde{t}_1}^2} [X_t + (2|h_t|^2 - \hat{g}^2) R'_t] \right\} \\ &+ \frac{3m_b^2}{8\pi^2} \left[ g(m_{\tilde{b}_1}^2, m_{\tilde{b}_2}^2) R_b (|h_b|^2 R_b - \tan\beta X_b) + \hat{g}^2 \tan\beta R_b \log \frac{m_{\tilde{b}_2}^2}{m_{\tilde{b}_1}^2} \right]. \end{aligned}$$

As analysis in Ref.[2], for above elements of the squared mass matrix, the input parameters can be chosen as  $m_A^2$ ,  $A_t \mu e^{i\xi}$  and  $A_b \mu e^{i\xi}$ , and there are only two CP violation phase angles:  $\kappa_1 = \theta_{A_t} + \theta_\mu + \xi$  and  $\kappa_2 = \theta_{A_b} + \theta_\mu + \xi$ . Therefore, it is equivalent that we choose  $\theta_{A_t}$  and  $\theta_{A_b}$  as the CP violation angles, and  $\theta_\mu = \xi = 0$ .

Diagonalizing the squared mass matrix of the neutral Higgs, we get the mass eigenstates  $h_1$ ,  $h_2$  and  $h_3$  of the Higgs bosons by the unitary matrix  $\mathcal{X}$ :

$$\mathcal{X} \mathcal{M}_H^2 \mathcal{X}^\dagger = (m_{h_1}^2, m_{h_2}^2, m_{h_3}^2), \quad (16)$$

with  $m_{h_1} \leq m_{h_2} \leq m_{h_3}$ . They are different from the CP eigenstates ( $h^0, H^0, A^0$ ). According to the above diagonalization procedure, we have

$$\begin{pmatrix} h_1 \\ h_2 \\ h_3 \end{pmatrix} = \mathcal{X} \begin{pmatrix} \phi_1 \\ \phi_2 \\ a \end{pmatrix}. \quad (17)$$

Using the relations[18]

$$\begin{pmatrix} h^0 \\ H^0 \end{pmatrix} = \begin{pmatrix} -\sin \alpha & \cos \alpha \\ \cos \alpha & \sin \alpha \end{pmatrix} \begin{pmatrix} \phi_1 \\ \phi_2 \end{pmatrix}, \quad (18)$$

we can get

$$\begin{pmatrix} h_1 \\ h_2 \\ h_3 \end{pmatrix} = \mathcal{X} \begin{pmatrix} -\sin \alpha & \cos \alpha & 0 \\ \cos \alpha & \sin \alpha & 0 \\ 0 & 0 & 1 \end{pmatrix} \begin{pmatrix} h^0 \\ H^0 \\ A^0 \end{pmatrix} = \mathcal{O} \begin{pmatrix} h^0 \\ H^0 \\ A^0 \end{pmatrix}. \quad (19)$$

Here  $\mathcal{O}$  is a unitary matrix, which translates ( $h^0, H^0, A^0$ ) into ( $h_1, h_2, h_3$ ).

In this paper, for simplicity, we assume that only squark sector has the complex parameters, and  $A_u = A_d = A_t = A_b = Ae^{i\theta_A}$  and  $\mu$  is real. Below we consider only the case of  $\theta_\mu = \xi = 0$  and  $\theta_A = \pi/2$ .

### III. CALCULATIONS OF ELECTRIC DIPOLE MOMENTS

The EDMs of electron, neutron, thallium and mercury may strongly constrain the explicit CP violation parameter space in the MSSM. Although it is supposed that cancelations possibly appear among many contributions [4, 11, 14, 19], it is still necessary to calculate the constraints on the parameter space of the explicit CP violation based on the recent detailed theoretical analysis[9, 10, 11, 12, 13, 14] so far.

In this section, we briefly summarize the present theoretical analysis on the EDMs and the chromoelectric dipole moments (CEDMs).

The one-loop contributions to the electron and quarks EDMs and CEDMs are given by[11]

$$d_{q-gluino}^E/e = -\frac{2\alpha_s}{3\pi} \sum_{k=1}^2 \text{Im}(\Gamma_q^{1k}) \frac{m_{\tilde{g}}}{M_{\tilde{q}_k}^2} Q_{\tilde{q}} \text{B}\left(\frac{m_{\tilde{g}}^2}{M_{\tilde{q}_k}^2}\right), \quad (20)$$

$$d_{f\text{-neutralino}}^E/e = \frac{\alpha_{EM}}{4\pi \sin^2 \theta_W} \sum_{k=1}^2 \sum_{i=1}^4 \text{Im}(\eta_{fik}) \frac{m_{\tilde{\chi}_i^0}}{M_{\tilde{f}k}^2} Q_{\tilde{f}} B\left(\frac{m_{\tilde{\chi}_i^0}^2}{M_{\tilde{f}k}^2}\right), \quad (21)$$

$$d_{u\text{-chargino}}^E/e = \frac{-\alpha_{EM}}{4\pi \sin^2 \theta_W} \sum_{k=1}^2 \sum_{i=1}^2 \text{Im}(\Gamma_{uik}) \frac{m_{\tilde{\chi}_i^+}}{M_{\tilde{d}k}^2} [Q_{\tilde{d}} B\left(\frac{m_{\tilde{\chi}_i^+}^2}{M_{\tilde{d}k}^2}\right) + (Q_u - Q_{\tilde{d}}) A\left(\frac{m_{\tilde{\chi}_i^+}^2}{M_{\tilde{d}k}^2}\right)], \quad (22)$$

$$d_{d\text{-chargino}}^E/e = \frac{-\alpha_{EM}}{4\pi \sin^2 \theta_W} \sum_{k=1}^2 \sum_{i=1}^2 \text{Im}(\Gamma_{dik}) \frac{m_{\tilde{\chi}_i^+}}{M_{\tilde{u}k}^2} [Q_{\tilde{u}} B\left(\frac{m_{\tilde{\chi}_i^+}^2}{M_{\tilde{u}k}^2}\right) + (Q_d - Q_{\tilde{u}}) A\left(\frac{m_{\tilde{\chi}_i^+}^2}{M_{\tilde{u}k}^2}\right)], \quad (23)$$

$$d_{e\text{-chargino}}^E/e = \frac{\alpha_{EM}}{4\pi \sin^2 \theta_W} \frac{\kappa_e}{m_{\tilde{\nu}_e}^2} \sum_{i=1}^2 m_{\tilde{\chi}_i^+} \text{Im}(U_{i2}^* V_{i1}) A\left(\frac{m_{\tilde{\chi}_i^+}^2}{m_{\tilde{\nu}_e}^2}\right), \quad (24)$$

$$\tilde{d}_{q\text{-gluino}}^C = \frac{g_s \alpha_s}{4\pi} \sum_{k=1}^2 \text{Im}(\Gamma_q^{1k}) \frac{m_{\tilde{g}}}{M_{\tilde{q}k}^2} C\left(\frac{m_{\tilde{g}}^2}{M_{\tilde{q}k}^2}\right), \quad (25)$$

$$\tilde{d}_{q\text{-neutralino}}^C = \frac{g_s g^2}{16\pi^2} \sum_{k=1}^2 \sum_{i=1}^4 \text{Im}(\eta_{qik}) \frac{m_{\tilde{\chi}_i^0}}{M_{\tilde{q}k}^2} B\left(\frac{m_{\tilde{\chi}_i^0}^2}{M_{\tilde{q}k}^2}\right), \quad (26)$$

$$\tilde{d}_{q\text{-chargino}}^C = \frac{-g^2 g_s}{16\pi^2} \sum_{k=1}^2 \sum_{i=1}^2 \text{Im}(\Gamma_{qik}) \frac{m_{\tilde{\chi}_i^+}}{M_{\tilde{q}k}^2} B\left(\frac{m_{\tilde{\chi}_i^+}^2}{M_{\tilde{q}k}^2}\right), \quad (27)$$

where the definitions of A, B, C,  $\Gamma_q^{1k}$ ,  $\eta_{fik}$  and  $\Gamma_{qik}$ , and their expressions are given explicitly in Appendix.

Using the naive dimensional analysis[20], the contributions from the CEDMs at the electroweak scale are

$$d_q^C = \frac{e}{4\pi} \tilde{d}_q^C \eta^C. \quad (28)$$

The two-loop contributions to the EDMs and CEDMs are given by[13]

$$\left(\frac{d_f}{e}\right)^\gamma = Q_f \frac{N_c \alpha \tan \beta m_f}{32\pi^3 M_a^2} \sum_{q=t,b} \xi_q Q_q^2 \left[ F\left(\frac{M_{\tilde{q}_1}^2}{M_a^2}\right) - F\left(\frac{M_{\tilde{q}_2}^2}{M_a^2}\right) \right], \quad (29)$$

$$\left(\frac{d_f}{e}\right)^Z = -(I_{3L}^f - 2Q_f \sin^2 \theta_w) \frac{N_c \alpha_w \tan \beta m_f}{64 \cos^2 \theta_w \pi^3 M_a^2} \quad (30)$$

$$\times \sum_{q=t,b} \sum_{i,j=1,2} \frac{1}{v} \text{Re} \Gamma^{a\tilde{q}_i^* \tilde{q}_j} K_{ij}^q Q_q G\left(\frac{M_Z^2}{M_a^2}, \frac{M_{\tilde{q}_i}^2}{M_a^2}, \frac{M_{\tilde{q}_j}^2}{M_a^2}\right), \quad (31)$$

$$\left(\frac{d_f}{e}\right)^W = \frac{N_c \alpha_w \tan \beta m_f}{128\sqrt{2}\pi^3 M_{H^+}^2} \sum_{i,j=1,2} \frac{1}{v} \text{Im} \Gamma^{H^+ \tilde{t}_i^* \tilde{b}_j} K_{ij}^{tb} \quad (32)$$

$$\times \left[ Q_t G\left(\frac{M_W^2}{M_{H^+}^2}, \frac{M_{\tilde{t}_i}^2}{M_{H^+}^2}, \frac{M_{\tilde{b}_j}^2}{M_{H^+}^2}\right) + Q_b G\left(\frac{M_W^2}{M_{H^+}^2}, \frac{M_{\tilde{b}_i}^2}{M_{H^+}^2}, \frac{M_{\tilde{t}_j}^2}{M_{H^+}^2}\right) \right], \quad (33)$$

$$\left(\frac{d_f^C}{e}\right)^g = \frac{\alpha_s}{64\pi^3} \frac{\tan\beta m_f}{M_a^2} \sum_{q=t,b} \xi_q \left[ F\left(\frac{M_{\tilde{q}_1}^2}{M_a^2}\right) - F\left(\frac{M_{\tilde{q}_2}^2}{M_a^2}\right) \right], \quad (34)$$

where the definitions of F and G,  $Re\Gamma^{a\tilde{q}_i^*\tilde{q}_j}$ ,  $K_{ij}^q$ ,  $\xi_q$ ,  $Im\Gamma^{H^+\tilde{t}_i^*\tilde{b}_j}$  and  $K_{ij}^{tb}$ , and their explicit expressions are given in Appendix.

The atomic calculations[12, 21] have provided the expression of the thallium and the mercury EDMs:

$$d_{Tl} = -585d_e - e 43 \text{ GeV} \times (C_S^{sing} - 0.2C_S^{trip}), \quad (35)$$

$$\begin{aligned} d_{Hg} = & 7 \times 10^{-3} e (\tilde{d}_u - \tilde{d}_d) + 10^{-2} d_e \\ & -1.4 \times 10^{-5} e \text{ GeV}^2 \left( \frac{0.5C_{dd}}{m_d} + 3.3\kappa \frac{C_{sd}}{m_s} + \frac{C_{bd}}{m_b} (1 - 0.25\kappa) \right) \\ & +3.5 \times 10^{-3} \text{ GeV} e C_S + 4 \times 10^{-4} \text{ GeV} e C_P, \end{aligned} \quad (36)$$

where the definitions of  $C_S^{sing}$ ,  $C_S^{trip}$  and the Wilson coefficients are given explicitly in Appendix.

Using the QCD sum rule approaches[22], we can get the neutron EDM, combining the contributions from EDMs and CEDMs of u and d quarks and Weinberg operator, respectively.

$$d_n = d_n(d_q, \tilde{d}_q) + d_n(w) + d_n(C_{bd}), \quad (37)$$

where the three contributions are shown explicitly in Appendix, respectively.

#### IV. HIGGS PRODUCTIONS ASSOCIATED WITH SQUARK PAIRS

In this section, we investigate the neutral Higgs productions associated with the squark pairs at LHC in the MSSM with the explicit CP violation, and compare with the productions with the CP conservation. The dominant contributions are from the gluon-gluon fusion

$$g + g \rightarrow \tilde{q}_i + \tilde{q}_j^* + \Phi, \quad (38)$$

where  $q = t, b$ ,  $i, j = 1, 2$ ,  $\Phi = h_{1,2,3}$  for the explicit CP violation and  $\Phi = h^0, H^0, A^0$  for the CP conservation. Fig.1 shows the relevant Feynman diagrams at the leading-order.

The vertexes involved in our calculations are

$$\mathcal{L}_{\tilde{q}\tilde{q}g} = ig_s T_{rs}^a \delta_{ij} G_\mu^a \tilde{q}_{jr}^* \overleftrightarrow{\partial}^\mu \tilde{q}_{is}, \quad (39)$$

$$\mathcal{L}_{\tilde{q}\tilde{q}gg} = \frac{1}{2}g_s^2\left(\frac{1}{3}\delta_{ab} + d_{abc}T^c\right)\delta_{ij}G_\mu^a G^{b\mu}\tilde{q}_j^*\tilde{q}_i, \quad (40)$$

$$\mathcal{L}_{ggg} = -\frac{1}{2}g_s f^{abc}(\partial_\mu G_\nu^a - \partial_\nu G_\mu^a)G^{b\mu}G^{c\nu}, \quad (41)$$

$$\mathcal{L}_{\tilde{q}\tilde{q}\Phi} = (G_k^{\tilde{q}})_{ij}\Phi_k\tilde{q}_j^{a*}\tilde{q}_i^a \quad (42)$$

for  $\Phi_k = (h^0, H^0, A^0)$ , and

$$\mathcal{L}_{\tilde{q}\tilde{q}\Phi} = \left[ \sum_{m=1}^3 \mathcal{O}_{km}(G_m^{\tilde{q}})_{ij} \right] \Phi_k\tilde{q}_j^{a*}\tilde{q}_i^a \quad (43)$$

for  $\Phi_k = h_k (k = 1, 2, 3)$ ,

with

$$A \overleftrightarrow{\partial}_\mu B = A(\partial_\mu B) - (\partial_\mu A)B, \quad (44)$$

$$G_k^{\tilde{q}} = \mathcal{R}^{\tilde{q}}\hat{G}_k^{\tilde{q}}(\mathcal{R}^{\tilde{q}})^\dagger, \quad (45)$$

$$(G_k^{\tilde{q}})_{ij} = \left[ \mathcal{R}^{\tilde{q}}\hat{G}_k^{\tilde{q}}(\mathcal{R}^{\tilde{q}})^\dagger \right]_{ij}, \quad (46)$$

$$\hat{G}_1^{\tilde{q}} = \begin{pmatrix} \frac{gm_Z}{c_W}(I_{3L}^q - e_q s_W^2)s_{\alpha+\beta} - \sqrt{2}m_q h_q \left\{ \begin{smallmatrix} c_\alpha \\ -s_\alpha \end{smallmatrix} \right\} & -\frac{1}{\sqrt{2}}h_q(A_q \left\{ \begin{smallmatrix} c_\alpha \\ -s_\alpha \end{smallmatrix} \right\} + \mu \left\{ \begin{smallmatrix} s_\alpha \\ -c_\alpha \end{smallmatrix} \right\}) \\ \frac{1}{\sqrt{2}}h_q(A_q \left\{ \begin{smallmatrix} c_\alpha \\ -s_\alpha \end{smallmatrix} \right\} + \mu \left\{ \begin{smallmatrix} s_\alpha \\ -c_\alpha \end{smallmatrix} \right\}) & \frac{gm_Z}{c_W}e_q s_W^2 s_{\alpha+\beta} - \sqrt{2}m_q h_q \left\{ \begin{smallmatrix} c_\alpha \\ -s_\alpha \end{smallmatrix} \right\} \end{pmatrix}, \quad (47)$$

$$\hat{G}_2^{\tilde{q}} = \begin{pmatrix} -\frac{gm_Z}{c_W}(I_{3L}^q - e_q s_W^2)c_{\alpha+\beta} - \sqrt{2}m_q h_q \left\{ \begin{smallmatrix} s_\alpha \\ c_\alpha \end{smallmatrix} \right\} & -\frac{1}{\sqrt{2}}h_q(A_q \left\{ \begin{smallmatrix} s_\alpha \\ c_\alpha \end{smallmatrix} \right\} - \mu \left\{ \begin{smallmatrix} c_\alpha \\ s_\alpha \end{smallmatrix} \right\}) \\ -\frac{1}{\sqrt{2}}h_q(A_q \left\{ \begin{smallmatrix} s_\alpha \\ c_\alpha \end{smallmatrix} \right\} - \mu \left\{ \begin{smallmatrix} c_\alpha \\ s_\alpha \end{smallmatrix} \right\}) & -\frac{gm_Z}{c_W}e_q s_W^2 c_{\alpha+\beta} - \sqrt{2}m_q h_q \left\{ \begin{smallmatrix} s_\alpha \\ c_\alpha \end{smallmatrix} \right\} \end{pmatrix}, \quad (48)$$

$$\hat{G}_3^{\tilde{q}} = i\frac{gm_q}{2m_W} \begin{pmatrix} 0 & -A_q \left\{ \begin{smallmatrix} \cot\beta \\ \tan\beta \end{smallmatrix} \right\} - \mu \\ A_q \left\{ \begin{smallmatrix} \cot\beta \\ \tan\beta \end{smallmatrix} \right\} + \mu & 0 \end{pmatrix}, \quad (49)$$

where  $\{\}$  represents  $\left\{ \begin{smallmatrix} up \\ down \end{smallmatrix} \right\}$  type squarks, respectively,  $T$  is the  $3 \times 3$   $SU(3)$  color matrix,  $d^{abc}$  are the  $SU(3)$  structure constants,  $f^{abc}$  are the  $SU(3)$  antisymmetric structure constants, and  $c_W \equiv \cos \theta_W$ ,  $s_W \equiv \sin \theta_W$ ,  $s_\alpha \equiv \sin \alpha$ ,  $c_\alpha \equiv \cos \alpha$ ,  $c_{\alpha+\beta} \equiv \cos(\alpha + \beta)$  and  $s_{\alpha+\beta} \equiv \sin(\alpha + \beta)$ .

We use the notations  $m_3 = m_{\tilde{q}_i^c}$  and  $m_5 = m_{\tilde{q}_j^{d*}}$  for the squark masses, the Mandelstam variables  $s_{ij} = (p_i + p_j)^2$  and  $t_{ij} = (p_i - p_j)^2$ , and define  $\Gamma_3$  and  $\Gamma_5$  as the decay widths of  $\tilde{q}_i^c$  and  $\tilde{q}_j^{d*}$ , respectively. Then the amplitudes for the process

$$g^a(p_1)g^b(p_2) \rightarrow \tilde{q}_i^c(p_3)\tilde{q}_j^{d*}(p_5)\Phi_k(p_4) \quad (50)$$

are given by

$$\mathcal{M}^{abcd} = \sum_{i=1}^{10} \mathcal{M}_i^{abcd}, \quad (51)$$

where  $\mathcal{M}_i^{abcd}$  ( $i = 1, \dots, 10$ ) represent the different contributions from the individual Feynman diagrams in Fig.1. Their explicit expressions are

$$\mathcal{M}_1^{abcd} = - \sum_{\mu} C_{\mu}^{\mu} \frac{1}{2} \left( \frac{1}{3} \delta_{ab} \mathbb{I}^8 + \sum_f d_{abf} \mathbb{T}^f \right)^{cd} \frac{1}{s_{34} - m_5^2 + i\Gamma_5 m_5}, \quad (52)$$

$$\mathcal{M}_2^{abcd} = - \sum_{\mu} C_{\mu}^{\mu} \frac{1}{2} \left( \frac{1}{3} \delta_{ab} \mathbb{I}^8 + \sum_f d_{abf} \mathbb{T}^f \right)^{cd} \frac{1}{s_{45} - m_3^2 + i\Gamma_3 m_3}, \quad (53)$$

$$\mathcal{M}_3^{abcd} = \sum_{\mu, \nu, \rho, e} C^{\mu\nu} f^{abe} T_{cd}^e V_{\mu\nu\rho}(p_1, p_2, -p_1 - p_2) \frac{(p_3 + p_4 - p_5)^\rho}{s_{12}(s_{34} - m_5^2 + i\Gamma_5 m_5)}, \quad (54)$$

$$\mathcal{M}_4^{abcd} = \sum_{\mu, \nu, \rho, e} C^{\mu\nu} f^{abe} T_{cd}^e V_{\mu\nu\rho}(p_1, p_2, -p_1 - p_2) \frac{(p_3 - p_4 - p_5)^\rho}{s_{12}(s_{45} - m_3^2 + i\Gamma_3 m_3)}, \quad (55)$$

$$\mathcal{M}_5^{abcd} = \sum_{\mu, \nu, e} C^{\mu\nu} T_{ce}^a T_{ed}^b \frac{(2p_3 - p_1)_\mu (p_2 - 2p_5)_\nu}{(t_{13} - m_3^2 + i\Gamma_3 m_3)(t_{25} - m_5^2 + i\Gamma_5 m_5)}, \quad (56)$$

$$\mathcal{M}_6^{abcd} = \sum_{\mu, \nu, e} C^{\mu\nu} T_{ed}^a T_{ce}^b \frac{(p_1 - 2p_5)_\mu (2p_3 - p_2)_\nu}{(t_{15} - m_5^2 + i\Gamma_5 m_5)(t_{23} - m_3^2 + i\Gamma_3 m_3)}, \quad (57)$$

$$\mathcal{M}_7^{abcd} = \sum_{\mu, \nu, e} C^{\mu\nu} T_{ce}^a T_{ed}^b \frac{(p_2 + p_3 + p_4 - p_5)_\mu (p_2 - 2p_5)_\nu}{(s_{34} - m_5^2 + i\Gamma_5 m_5)(t_{25} - m_5^2 + i\Gamma_5 m_5)}, \quad (58)$$

$$\mathcal{M}_8^{abcd} = \sum_{\mu, \nu, e} C^{\mu\nu} T_{ce}^a T_{ed}^b \frac{(2p_3 - p_1)_\mu (p_3 - p_1 - p_4 - p_5)_\nu}{(s_{45} - m_3^2 + i\Gamma_3 m_3)(t_{13} - m_3^2 + i\Gamma_3 m_3)}, \quad (59)$$

$$\mathcal{M}_9^{abcd} = \sum_{\mu, \nu, e} C^{\mu\nu} T_{ed}^a T_{ce}^b \frac{(p_1 - 2p_5)_\mu (p_1 + p_3 + p_4 - p_5)_\nu}{(s_{34} - m_5^2 + i\Gamma_5 m_5)(t_{15} - m_5^2 + i\Gamma_5 m_5)}, \quad (60)$$

$$\mathcal{M}_{10}^{abcd} = \sum_{\mu, \nu, e} C^{\mu\nu} T_{ed}^a T_{ce}^b \frac{(p_3 - p_2 - p_4 - p_5)_\mu (2p_3 - p_2)_\nu}{(s_{45} - m_3^2 + i\Gamma_3 m_3)(t_{23} - m_3^2 + i\Gamma_3 m_3)}, \quad (61)$$

where  $C^{\mu\nu} = ig_s^2 \epsilon^\mu(p_1) \epsilon^\nu(p_2) D_{kji}^{\tilde{q}}$ ,  $V_{\mu_1\mu_2\mu_3}(k_1, k_2, k_3) = (k_1 - k_2)_{\mu_3} g_{\mu_1\mu_2} + (k_2 - k_3)_{\mu_1} g_{\mu_2\mu_3} + (k_3 - k_1)_{\mu_2} g_{\mu_3\mu_1}$ , and

$$D_{kij}^{\tilde{q}} = \begin{cases} (G_k^{\tilde{q}})_{ij}, & \text{for CPC,} \\ \sum_{m=1}^3 \mathcal{O}_{km} (G_m^{\tilde{q}})_{ij}, & \text{for CPV.} \end{cases} \quad (62)$$

The averaged amplitude square is

$$|\mathcal{M}|_{avg}^2 = \frac{1}{256} \sum_{a,b,c,d} |\mathcal{M}^{abcd}|^2. \quad (63)$$

Then the partonic cross sections are

$$\hat{\sigma} = \int \frac{1}{2s} |\mathcal{M}|_{avg}^2 dPS, \quad (64)$$

where  $dPS$  represents the phase space integration variables.

Considering the  $pp$  collision at the LHC, the total cross sections are given by

$$\sigma = \int_{\tau}^1 dx_1 \int_{\tau/x_1}^1 dx_2 f_1(x_1) f_2(x_2) \hat{\sigma}(s = x_1 x_2 S), \quad (65)$$

where  $f_1(x_1)$  and  $f_2(x_2)$  are parton distribution functions (PDFs), and  $\tau = (m_{\tilde{q}} + m_{\tilde{q}'} + m_{\Phi})^2/S$ .

## V. NUMERICAL RESULTS AND DISCUSSIONS

In our numerical calculations, the Standard Model parameters are chosen to be  $\alpha_{ew}(m_W) = 1/137$ ,  $m_Z = 91.1875$  GeV,  $m_W = 80.45$  GeV and  $m_t = 174$  GeV[27]. We used the CTEQ6M PDFs[25] and the two-loop evaluation for  $\alpha_s(Q)$ [23] ( $\alpha_s(m_Z) = 0.118$ ) and the running bottom quark mass[24].

The other Standard Model input parameters are[26, 27]

$$\begin{aligned} m_e &= 0.51 \text{ MeV}, & m_\mu &= 105.658 \text{ MeV}, & m_\tau &= 1.777 \text{ GeV}, \\ m_d &= 4 \text{ MeV}, & m_s &= 120 \text{ MeV}, & m_b &= 4.2 \text{ GeV}, \\ m_u &= 2.5 \text{ MeV}, & m_c &= 1.2 \text{ GeV}. \end{aligned} \quad (66)$$

In addition, we assumed that the complex parameters only exist in the squark sector. For simplicity, we chose  $A_t = A_b = A_u = A_d = Ae^{i\theta_A}$  and  $m_{\tilde{Q}} = m_{\tilde{U}} = m_{\tilde{D}} = m_{\tilde{E}} = m_{\tilde{L}} = M_{SUSY}$ . Then the solution of  $m_{\tilde{t}_1}$  in Eq.(10) became

$$m_{\tilde{t}_1}^2 = M_{SUSY}^2 + \frac{1}{2} |h_t|^2 v_2^2 - \frac{\hat{g}}{4} (v_2^2 - v_1^2) - \frac{1}{2} \sqrt{\left( \frac{3g_2^2 - 5g_1^2}{24} \mathcal{D} \right)^2 + 2|h_t|^2 |A_t v_2 + \mu v_1|^2}. \quad (67)$$

Using this expression, we chose  $m_{\tilde{t}_1}$  as the input parameter instead of  $M_{SUSY}$ .

The other MSSM input parameters are fixed as following:

$$M_1 = 100\text{GeV}, \quad M_2 = 200\text{GeV}, \quad M_3 = 300\text{GeV}, \quad A_t = A_\tau = 1000\text{GeV}, \quad \theta_A = \pi/2. \quad (68)$$

The remaining MSSM input parameters are  $\tan\beta$ ,  $m_{A^0}$ ,  $m_{\tilde{t}_1}$ ,  $A$  and  $\mu$ .

### A. PARAMETER SPACE CONSTRAINTS

The strongest constraints on the CP violation parameters arise from the experiments on the atomic EDMs of thallium[6] and mercury[7] and that of neutron[5]:

$$\begin{aligned} |d_{\text{Tl}}| &< 9 \times 10^{-25} e \text{ cm}, \\ |d_{\text{Hg}}| &< 2 \times 10^{-28} e \text{ cm}, \\ |d_n| &< 6 \times 10^{-26} e \text{ cm}, \end{aligned} \quad (69)$$

and the measurement of  $d_{Tl}$  can be translated into a tight bound,  $|d_e| < 1.6 \times 10^{-27} e \text{ cm}$ [10]. Besides the EDMs experiments, the bounds on the Higgs and squarks masses should also be considered. The current lower mass bounds[26, 27] on the neutral Higgs, the stop and the sbottom are 89.8 GeV, 95.7 GeV and 89 GeV, respectively, and in order to avoid a color breaking VEV,  $|A_t|$  and  $|A_b|$  could not be too large[15, 28]:

$$\begin{aligned} |A_t|^2 &< 3(m_{Q_3}^2 + m_{U_3^c}^2 + m_2^2), \\ |A_b|^2 &< 3(m_{Q_3}^2 + m_{D_3^c}^2 + m_1^2). \end{aligned} \quad (70)$$

Combining all the above constraints, we can obtain the allowed areas in the parameter spaces.

Figs.2-4 show the allowed ranges of the parameters  $A$  and  $\mu$ , taking different  $\tan\beta$ ,  $m_{\tilde{t}_1}$ ,  $M_{A^0}$ , respectively. In general, the parameters  $\mu$  and  $A$  are constrained more stringently for small  $M_{A^0}$ , and the constraints on both  $A$  and  $\mu$  are weakened for larger  $m_{\tilde{t}_1}$ . Besides, the allowed ranges of  $\mu$  are sharply constrained for large  $\tan\beta$ . When  $\tan\beta > 25$ , the parameters  $\mu$  and  $A$  are almost forbidden. We will mainly consider the case of  $\tan\beta \geq 5$  and  $M_{A^0} = 300 \text{ GeV}$  in the following.

Fig.5 gives the allowed ranges of the parameters  $\tan\beta$  and  $m_{\tilde{t}_1}$ , taking different values of  $A = 900 \text{ GeV}$ ,  $500 \text{ GeV}$  and  $\mu = 400 \text{ GeV}$ ,  $700 \text{ GeV}$ , respectively.  $\tan\beta$  can be strongly constrained for larger  $\mu$  and smaller  $A$ . For example, for  $A = 500 \text{ GeV}$  and  $\mu = 700 \text{ GeV}$ ,

$\tan\beta$  is almost limited near 5. Besides, in the case of  $\mu = 700$  GeV,  $m_{\tilde{t}_1}$  is strongly constrained only for large  $\tan\beta$ .

## B. HIGGS PRODUCTIONS ASSOCIATED WITH SQUARK PAIRS

Using the allowed ranges of the parameters mentioned above, we investigate the neutral Higgs productions associated with squarks pairs in the MSSM with the explicit CP violation and the CP conservation, respectively. In the experiments, the mass eigenstates of the Higgs bosons will be the observables, which are used to distinguish the different Higgs bosons, and for comparison with the case of the CPC, we will mainly focus on the productions of the lightest Higgs associated with squark pairs.

Fig.6 shows the total cross sections of two processes  $pp \rightarrow \tilde{q}_i \tilde{q}_j^* h^0$  and  $pp \rightarrow \tilde{q}_i \tilde{q}_j^* h_1$  as the functions of  $\tan\beta$ , respectively, assuming  $M_{A^0} = 300$  GeV,  $A = 900$  GeV,  $\mu = 400$  GeV,  $m_{\tilde{t}_1} = 100$  GeV or 200 GeV. In general, the total cross sections in the case of the CPV are larger than ones in the case of the CPC, especially for  $\tan\beta \approx 5$ . we can see that the total cross sections for  $\tilde{t}_1 \tilde{t}_1^* \Phi_1$  ( $\Phi_1 = h_1, h^0$ ) productions are the largest, which can reach

$$\sigma(h^0 \tilde{t}_1 \tilde{t}_1^*) \approx 2.55 pb \quad \text{and} \quad \sigma(h_1 \tilde{t}_1 \tilde{t}_1^*) \approx 3.78 pb, \quad (71)$$

respectively, for  $A = 900$  GeV,  $\mu = 400$  GeV,  $m_{\tilde{t}_1} = 100$  GeV and  $\tan\beta = 5$ . Note that  $\sigma(h_1 \tilde{t}_1 \tilde{t}_1^*)$  are enhanced by about 50%, compared with  $\sigma(h^0 \tilde{t}_1 \tilde{t}_1^*)$ . At the LHC, with an integrated luminosity of  $100 fb^{-1}$  (i.e.,  $\int L dt = 100 fb^{-1}$ ), we can expect that the events will be  $2.55 \times 10^5$  for  $\sigma(h^0 \tilde{t}_1 \tilde{t}_1^*)$  and  $3.78 \times 10^5$  for  $\sigma(h_1 \tilde{t}_1 \tilde{t}_1^*)$ , respectively, and those signals may be observable. From Fig.6, one also sees that all the total cross sections for  $m_{\tilde{t}_1} = 200$  GeV are generally less than ones for  $m_{\tilde{t}_1} = 100$  GeV.

In Fig.7, we plots the total cross sections of two processes  $pp \rightarrow \tilde{q}_i \tilde{q}_j^* H^0$  and  $pp \rightarrow \tilde{q}_i \tilde{q}_j^* h_2$  as the functions of  $\tan\beta$ , respectively, assuming  $M_{A^0} = 300$  GeV,  $A = 900$  GeV,  $\mu = 400$  GeV,  $m_{\tilde{t}_1} = 100$  GeV or 200 GeV. From Fig.7, we find that the total cross sections for  $\tilde{t}_1 \tilde{t}_1^* H^0$  productions are larger than ones for  $\tilde{t}_1 \tilde{t}_1^* h_2$  productions, which of both processes can generally reach tens of fb.

Fig.8 shows the total cross sections  $\sigma(\tilde{q}_i \tilde{q}_j^* A^0)$  and  $\sigma(\tilde{q}_i \tilde{q}_j^* h_3)$  as the functions of  $\tan\beta$ , respectively, assuming  $M_{A^0} = 300$  GeV,  $A = 900$  GeV,  $\mu = 400$  GeV,  $m_{\tilde{t}_1} = 100$  GeV or 200 GeV, respectively. In the case of the CPC, there are only associated productions

$pp \rightarrow A^0 \tilde{t}_1 \tilde{t}_2^*$  and  $pp \rightarrow A^0 \tilde{b}_1 \tilde{b}_2^*$  because of the squarks-Higgs coupling structure. The cross sections  $\sigma(h_3 \tilde{t}_1 \tilde{t}_1^*)$ ,  $\sigma(h_3 \tilde{t}_1 \tilde{t}_2^*)$  and  $\sigma(A^0 \tilde{t}_1 \tilde{t}_2^*)$  are generally a few fb, and the other cross sections are less than 1fb.

From the above analysis, we can find that when  $\tan \beta = 5$  and  $m_{\tilde{t}_1} = 100$  GeV, the total cross sections in the most of the production channels are largest, and the dominant processes among those channels are  $pp \rightarrow \Phi_1 \tilde{t}_1 \tilde{t}_1^*$ . The relevant numerical results are shown in TABLE I and TABLE II for  $m_{\tilde{t}_1} = 100$  GeV and  $m_{\tilde{t}_1} = 150$  GeV, respectively.

TABLE I: The total cross sections for  $\tan \beta = 5$ ,  $M_{A^0} = 300$  GeV,  $m_{\tilde{t}_1} = 100$  GeV,  $A = 900$  GeV and  $\mu = 400$  GeV

$\Phi$	$h^0$	$H^0$	$A^0$	$h_1$	$h_2$	$h_3$
$\sigma(\tilde{b}_1 \tilde{b}_1^* \Phi)/fb$	$1.46 \times 10^{-4}$	$2.17 \times 10^{-2}$	0	$3.82 \times 10^{-2}$	$2.47 \times 10^{-2}$	$2.79 \times 10^{-3}$
$\sigma(\tilde{b}_1 \tilde{b}_2^* \Phi)/fb$	$2.76 \times 10^{-3}$	$4.07 \times 10^{-5}$	$2.04 \times 10^{-2}$	$1.72 \times 10^{-3}$	$2.23 \times 10^{-3}$	$1.96 \times 10^{-2}$
$\sigma(\tilde{b}_2 \tilde{b}_2^* \Phi)/fb$	$2.57 \times 10^{-2}$	$1.83 \times 10^{-2}$	0	0.116	$1.73 \times 10^{-2}$	$6.49 \times 10^{-4}$
$\sigma(\tilde{t}_1 \tilde{t}_1^* \Phi)/fb$	$2.55 \times 10^3$	56.7	0	$3.58 \times 10^3$	32.1	6.87
$\sigma(\tilde{t}_1 \tilde{t}_2^* \Phi)/fb$	$1.47 \times 10^{-3}$	$6.29 \times 10^{-5}$	12.3	1.67	2.02	4.88
$\sigma(\tilde{t}_2 \tilde{t}_2^* \Phi)/fb$	1.35	$5.77 \times 10^{-2}$	0	2.20	$2.47 \times 10^{-2}$	$1.66 \times 10^{-2}$

TABLE II: The total cross sections for  $\tan \beta = 5$ ,  $M_{A^0} = 300$  GeV,  $m_{\tilde{t}_1} = 150$  GeV,  $A = 900$  GeV and  $\mu = 400$  GeV

$\Phi$	$h^0$	$H^0$	$A^0$	$h_1$	$h_2$	$h_3$
$\sigma(\tilde{b}_1 \tilde{b}_1^* \Phi)/fb$	$1.06 \times 10^{-4}$	$1.76 \times 10^{-2}$	0	$2.86 \times 10^{-2}$	$1.86 \times 10^{-2}$	$2.94 \times 10^{-3}$
$\sigma(\tilde{b}_1 \tilde{b}_2^* \Phi)/fb$	$2.14 \times 10^{-3}$	$3.34 \times 10^{-5}$	$1.68 \times 10^{-2}$	$1.09 \times 10^{-3}$	$2.32 \times 10^{-3}$	$1.53 \times 10^{-2}$
$\sigma(\tilde{b}_2 \tilde{b}_2^* \Phi)/fb$	$2.04 \times 10^{-2}$	$1.53 \times 10^{-2}$	0	$8.55 \times 10^{-2}$	$1.34 \times 10^{-2}$	$8.28 \times 10^{-4}$
$\sigma(\tilde{t}_1 \tilde{t}_1^* \Phi)/fb$	504.1	16.6	0	621.3	9.20	1.64
$\sigma(\tilde{t}_1 \tilde{t}_2^* \Phi)/fb$	$1.32 \times 10^{-3}$	$5.50 \times 10^{-5}$	10.8	1.51	1.38	4.32
$\sigma(\tilde{t}_2 \tilde{t}_2^* \Phi)/fb$	1.19	$5.21 \times 10^{-2}$	0	1.77	$2.17 \times 10^{-2}$	$1.33 \times 10^{-2}$

Fig.9 shows the curves of  $\sigma(\tilde{q}_i \tilde{q}_j^* h^0)$  and  $\sigma(\tilde{q}_i \tilde{q}_j^* h_1)$  as the functions of  $A$ , respectively, assuming  $M_{A^0} = 300$  GeV,  $\tan \beta = 5$ ,  $m_{\tilde{t}_1} = 100$  GeV and  $\mu = 400$  GeV or 1000 GeV. The dominant productions are still  $pp \rightarrow \Phi_1 \tilde{t}_1 \tilde{t}_1^*$ . In general, the total cross sections  $\sigma(h_1 \tilde{t}_1 \tilde{t}_1^*)$  are

enhanced, compared with  $\sigma(h^0\tilde{t}_1\tilde{t}_1^*)$ , and when  $A > 700$  GeV, such enhancements increase with increasing  $A$ . Especially, the enhancements can approach to infinite for some special values of  $A$  and  $\mu$ , because the total cross sections  $\sigma(h^0\tilde{t}_1\tilde{t}_1^*)$  approach to zero then, which arise from the squarks-Higgs couplings in the case of the CPC. For example,

$$\sigma(h^0\tilde{t}_1\tilde{t}_1^*) < 10^{-3} fb, \quad \sigma(h_1\tilde{t}_1\tilde{t}_1^*) \approx 270 fb, \quad (72)$$

for  $A = 568$  GeV and  $\mu = 1000$  GeV.

Fig.10 gives the total cross sections of two processes  $pp \rightarrow \tilde{q}_i\tilde{q}_j^*H^0$  and  $pp \rightarrow \tilde{q}_i\tilde{q}_j^*h_2$  as the functions of  $A$ , respectively, assuming  $M_{A^0} = 300$  GeV,  $\tan\beta = 5$ ,  $m_{\tilde{t}_1} = 100$  GeV and  $\mu = 400$  GeV or 1000 GeV. The total cross sections  $\sigma(\Phi_2\tilde{t}_1\tilde{t}_1^*)$  can reach hundreds of fb, corresponding to about  $10^4$  events at the LHC, while the other cross sections are generally less than 1fb.

Fig.11 shows the total cross sections of two processes  $pp \rightarrow \tilde{q}_i\tilde{q}_j^*A^0$  and  $pp \rightarrow \tilde{q}_i\tilde{q}_j^*h_3$  as the functions of  $A$ , respectively, assuming  $M_{A^0} = 300$  GeV,  $\tan\beta = 5$ ,  $m_{\tilde{t}_1} = 100$  GeV and  $\mu = 400$  GeV or 1000 GeV. From Fig.11, we can see that the total cross sections for  $\Phi_3\tilde{t}_1\tilde{t}_2^*(\Phi_3 = h_3, A^0)$  productions are the largest, which can reach hundreds of fb, but fastly decrease with increasing  $A$ .

Below, for comparison, we summarize some typical numerical results of the total cross sections of the processes  $pp \rightarrow \tilde{q}_i\tilde{q}_j^*\Phi$  in the MSSM without and with explicit CP violation in TABLE III and TABLE IV for  $m_{\tilde{t}_1} = 100$  GeV and  $m_{\tilde{t}_1} = 150$  GeV, respectively.

TABLE III: The total cross sections for  $\tan\beta = 5$ ,  $M_{A^0} = 300$  GeV,  $m_{\tilde{t}_1} = 100$  GeV,  $A = 568$  GeV and  $\mu = 1000$  GeV

$\Phi$	$h^0$	$H^0$	$A^0$	$h_1$	$h_2$	$h_3$
$\sigma(\tilde{b}_1\tilde{b}_1^*\Phi)/fb$	0.648	$3.82 \times 10^{-2}$	0	2.56	$6.48 \times 10^{-2}$	$1.30 \times 10^{-3}$
$\sigma(\tilde{b}_1\tilde{b}_2^*\Phi)/fb$	$5.56 \times 10^{-3}$	$4.87 \times 10^{-6}$	$2.64 \times 10^{-2}$	$1.0 \times 10^{-2}$	$5.76 \times 10^{-4}$	$3.07 \times 10^{-2}$
$\sigma(\tilde{b}_2\tilde{b}_2^*\Phi)/fb$	0.379	$1.86 \times 10^{-2}$	0	1.11	$2.18 \times 10^{-2}$	$2.79 \times 10^{-5}$
$\sigma(\tilde{t}_1\tilde{t}_1^*\Phi)/fb$	$1.51 \times 10^{-3}$	220.8	0	273.8	281.9	0.748
$\sigma(\tilde{t}_1\tilde{t}_2^*\Phi)/fb$	$6.84 \times 10^{-3}$	$5.16 \times 10^{-4}$	102.77	44.8	1.66	110.9
$\sigma(\tilde{t}_2\tilde{t}_2^*\Phi)/fb$	1.08	0.348	0	3.73	0.612	$1.79 \times 10^{-2}$

TABLE IV: The total cross sections for  $\tan \beta = 5$ ,  $M_{A^0} = 300$  GeV,  $m_{\tilde{t}_1} = 150$  GeV,  $A = 568$  GeV and  $\mu = 1000$  GeV

$\Phi$	$h^0$	$H^0$	$A^0$	$h_1$	$h_2$	$h_3$
$\sigma(\tilde{b}_1\tilde{b}_1^*\Phi)/fb$	0.447	$2.88 \times 10^{-2}$	0	1.63	$3.81 \times 10^{-2}$	$1.11 \times 10^{-3}$
$\sigma(\tilde{b}_1\tilde{b}_2^*\Phi)/fb$	$3.88 \times 10^{-3}$	$3.90 \times 10^{-6}$	$2.06 \times 10^{-2}$	$6.42 \times 10^{-3}$	$4.99 \times 10^{-4}$	$2.24 \times 10^{-2}$
$\sigma(\tilde{b}_2\tilde{b}_2^*\Phi)/fb$	0.292	$1.52 \times 10^{-2}$	0	1.11	$1.46 \times 10^{-2}$	$7.36 \times 10^{-6}$
$\sigma(\tilde{t}_1\tilde{t}_1^*\Phi)/fb$	$1.73 \times 10^{-3}$	64.4	0	62.3	69.7	0.110
$\sigma(\tilde{t}_1\tilde{t}_2^*\Phi)/fb$	$6.43 \times 10^{-3}$	$4.43 \times 10^{-4}$	89.56	39.5	0.723	75.2
$\sigma(\tilde{t}_2\tilde{t}_2^*\Phi)/fb$	0.92	0.307	0	3.20	0.472	$1.26 \times 10^{-2}$

In conclusion, we have calculated the total cross sections of the neutral Higgs productions associated with squark pairs in the MSSM without and with explicit CP violation, respectively. The dominant productions in both cases are always  $pp \rightarrow \Phi_1\tilde{t}_1\tilde{t}_1^*$ , which can reach a few pb, while the maximum results in Ref.[15] in the same final states are less than 500fb. In most of the parameter space, the total cross sections  $\sigma(\tilde{t}_1\tilde{t}_1^*h_1)$  are always significantly enhanced, compared with  $\sigma(\tilde{t}_1\tilde{t}_1^*h^0)$ . For some special parameters, the enhancements of a few order of magnitudes can be obtained.

### Acknowledgments

This work was supported in part by the National Natural Science Foundation of China, under Grant Nos. 10421503 and 10575001, and the key Grant Project of Chinese Ministry of Education, under Grant No. 305001.

### APPENDIX

In this appendix, we present the notations and definitions in the expressions of the EDM and CEDM [9, 10, 11, 12, 13, 14] in Section III.

The notations in the expressions of the one-loop contributions to the electron and quark EDMs and CEDMs, Eqs.(20)-(27), are given by

$$A(r) = \frac{1}{2(1-r)^2} \left( 3 - r + \frac{2 \ln r}{1-r} \right), \quad (73)$$

$$B(r) = \frac{1}{2(r-1)^2} \left( 1 + r + \frac{2r \ln r}{1-r} \right), \quad (74)$$

$$C(r) = \frac{1}{6(r-1)^2} \left( 10r - 26 + \frac{2r \ln r}{1-r} - \frac{18 \ln r}{1-r} \right), \quad (75)$$

$$\Gamma_q^{1k} = \mathcal{R}_{qk2}^* \mathcal{R}_{qk1}, \quad (76)$$

$$\eta_{fik} = [-\sqrt{2} \{ \tan \theta_W (Q_f - I_{3L}^f) N_{1i} + I_{3L}^f N_{2i} \} \mathcal{R}_{fk1} - \kappa_f N_{bi} \mathcal{R}_{fk2}] \quad (77)$$

$$\times (\sqrt{2} \tan \theta_W Q_f N_{1i} \mathcal{R}_{fk2}^* - \kappa_f N_{bi} \mathcal{R}_{fk1}^*), \quad (78)$$

$$\kappa_u = \frac{m_u}{\sqrt{2} m_W \sin \beta}, \quad (79)$$

$$\kappa_{d,e} = \frac{m_{d,e}}{\sqrt{2} m_W \cos \beta}, \quad (80)$$

$$\Gamma_{uik} = \kappa_u V_{i2}^* \mathcal{R}_{dk1}^* (U_{i1}^* \mathcal{R}_{dk1} - \kappa_d U_{i2}^* \mathcal{R}_{dk2}), \quad (81)$$

$$\Gamma_{dik} = \kappa_d U_{i2}^* \mathcal{R}_{uk1}^* (V_{i1}^* \mathcal{R}_{uk1} - \kappa_u V_{i2}^* \mathcal{R}_{uk2}), \quad (82)$$

where  $m_{\tilde{g}}$  is the gluino mass,  $N$  is the neutralino rotation matrix, and  $b = 3(4)$  for  $I_{3L}^f = -\frac{1}{2}(\frac{1}{2})$ .

The notations in the expressions of the two-loop contributions to the electron and quarks EDMs and CEDMs, Eqs.(29)-(34), are given by

$$F(z) = \int_0^1 dx \frac{x(1-x)}{z-x(1-x)} \ln \left[ \frac{x(1-x)}{z} \right], \quad (83)$$

$$G(a, b, c) = \int_0^1 dx x \left[ \frac{ax(1-x) \ln a}{(a-1)[ax(1-x) - bx - c(1-x)]} + \frac{x(1-x)[bx + c(1-x)]}{[ax(1-x) - bx - c(1-x)][x(1-x) - bx - c(1-x)]} \ln \left( \frac{bx + c(1-x)}{x(1-x)} \right) \right], \quad (84)$$

$$\xi_q = R_q \frac{\sin 2\theta_q m_q \text{Im}(\mu e^{i\delta_q})}{\sin \beta \cos \beta v^2}, \quad (85)$$

$$v^2 = v_1^2 + v_2^2 = M_Z^2/\hat{g}^2, \quad (86)$$

$$\text{Re } \Gamma^{a\tilde{q}_i^* \tilde{q}_j} = v \xi_q \begin{pmatrix} 1 & -\cot 2\theta_q \\ -\cot 2\theta_q & -1 \end{pmatrix}, \quad (87)$$

$$\begin{aligned} \text{Im } \Gamma^{H^+ \tilde{t}_i^* \tilde{b}_j} &= \frac{v}{\sqrt{2}} \begin{pmatrix} -\frac{\cos \theta_t}{\cos \theta_b} \xi_b + \frac{\cos \theta_b}{\cos \theta_t} \xi_t & \frac{\cos \theta_t}{\sin \theta_b} \xi_b + \frac{\sin \theta_b}{\cos \theta_t} \xi_t \\ -\frac{\sin \theta_t}{\cos \theta_b} \xi_b - \frac{\cos \theta_b}{\sin \theta_t} \xi_t & \frac{\sin \theta_t}{\sin \theta_b} \xi_b - \frac{\sin \theta_b}{\sin \theta_t} \xi_t \end{pmatrix} \\ &+ \frac{\sqrt{2} m_b m_t \sin(\delta_b - \delta_t)}{\sin \beta \cos \beta v^2} \begin{pmatrix} \sin \theta_t \sin \theta_b & -\sin \theta_t \cos \theta_b \\ -\cos \theta_t \sin \theta_b & \cos \theta_t \cos \theta_b \end{pmatrix}, \end{aligned} \quad (88)$$

$$K^q = \begin{pmatrix} 2I_{3L}^q \cos^2 \theta_q - 2Q_q \sin^2 \theta_w & I_{3L}^q \sin 2\theta_q \\ I_{3L}^q \sin 2\theta_q & 2I_{3L}^q \sin^2 \theta_q - 2Q_q \sin^2 \theta_w \end{pmatrix}, \quad (89)$$

$$K^{tb} = \begin{pmatrix} \cos \theta_t \cos \theta_b & \cos \theta_t \sin \theta_b \\ \sin \theta_t \cos \theta_b & \sin \theta_t \sin \theta_b \end{pmatrix}. \quad (90)$$

The notations in the expressions of the thallium and the mercury EDMs, Eqs.(35) and (36), are given by

$$C_S^{sing} = C_{de} \frac{29 \text{ MeV}}{m_d} + C_{se} \frac{\kappa \times 220 \text{ MeV}}{m_s} + C_{be} \frac{66 \text{ MeV}(1 - 0.25\kappa)}{m_b}, \quad (91)$$

$$C_S^{trip} \sim -C_{de} \frac{1 - 3 \text{ MeV}}{m_d}, \quad (92)$$

$$\kappa = 0.5. \quad (93)$$

In above expressions,  $C_{ij}(i, j = e, d, s, b)$  are the Wilson coefficients, which are given by

$$C_{ij}^{(vc)} = -\frac{\tan^2 \beta}{2m_A^2} \frac{Y_i^{SM} Y_j^{SM} \sin(\delta_i - \delta_j)}{|1 + \Delta m_i/m_i^{(0)}| |1 + \Delta m_j/m_j^{(0)}|}, \quad (94)$$

$$C_{ij}^{(AH)} \simeq \frac{\langle AH \rangle \tan^2 \beta}{2m_A^4} \frac{Y_i^{SM} Y_j^{SM}}{|1 + \Delta m_i/m_i^{(0)}| |1 + \Delta m_j/m_j^{(0)}|}, \quad (95)$$

with

$$\begin{aligned} \langle AH \rangle &= \frac{3}{8\pi^2 v^2} \left[ \frac{m_t^4 |\mu|^2 |A_t|^2}{(m_{t_1}^2 - m_{t_2}^2)^2} E(m_{t_2}^2/m_{t_1}^2) \sin(2\theta_{A_t} + 2\theta_\mu) \right. \\ &+ \frac{m_b^4 |\mu|^2 |A_b|^2 \tan^4 \beta}{(m_{b_1}^2 - m_{b_2}^2)^2} E(m_{b_2}^2/m_{b_1}^2) \sin(2\theta_{A_\tau} + 2\theta_\mu) \\ &\left. + \frac{m_\tau^4 |\mu|^2 |A_\tau|^2 \tan^4 \beta}{3(m_{\tau_1}^2 - m_{\tau_2}^2)^2} E(m_{\tau_2}^2/m_{\tau_1}^2) \sin(2\theta_{A_\tau} + 2\theta_\mu) \right], \end{aligned} \quad (96)$$

where Eq.(94) and Eq.(96) represent the contributions from the different diagrams, respectively, and  $Y_f^{SM} = \sqrt{2}m_f/v$  are the Standard Model values for the Yukawa couplings,  $m_i^{(0)} = Y_i^{(0)}v_1/\sqrt{2}$  are the tree-level fermion masses. Moreover,  $\delta_i = \delta_i^{(m)} - \delta_i^{(H)}$ , and for large  $\tan\beta$ ,  $\delta_i^{(H)} \ll \delta_i^{(m)}$ , and at one-loop level,  $\delta_i^{(m)} = \text{Arg}(1 + \Delta m_i/m_i^{(0)})$ . Here the corrections to the masses are given by

$$\begin{aligned}
(\Delta m_d)_{\lambda_3} &= \frac{2\alpha_s}{3\pi} e^{-i(\phi_d+\phi_3)} s_d c_d m_3 (m_{\tilde{d}_1}^2 - m_{\tilde{d}_2}^2) I(m_{\tilde{d}_1}^2, m_{\tilde{d}_2}^2, m_3^2), \\
(\Delta m_d)_{\chi^+} &= -\frac{\alpha_W m_d}{4\sqrt{2}\pi m_W \cos\beta} \sum_i U_{i2}^* V_{i1}^* m_{\chi_i^+} \left[ c_u^2 \tilde{B}_0(m_{\tilde{u}_1}^2, m_{\chi_i^+}^2) + s_u^2 \tilde{B}_0(m_{\tilde{u}_2}^2, m_{\chi_i^+}^2) \right], \\
(\Delta m_d)_{\chi^0} &= -\frac{\alpha_W}{36\pi} e^{-i\phi_d} \tan\theta_W s_d c_d (m_{\tilde{d}_1}^2 - m_{\tilde{d}_2}^2) \sum_i N_{i1}^* (N_{i1}^* \tan\theta_W - 3N_{i2}^*) m_{\chi_i^0} \\
&\quad \times I(m_{\tilde{d}_1}^2, m_{\tilde{d}_2}^2, m_{\chi_i^0}^2) \\
&\quad + \frac{\alpha_W m_d}{24\pi m_W \cos\beta} \sum_i N_{i3}^* (N_{i1}^* \tan\theta_W - 3N_{i2}^*) m_{\chi_i^0} \left[ c_d^2 \tilde{B}_0(m_{\tilde{d}_1}^2, m_{\chi_i^0}^2) \right. \\
&\quad \left. + s_d^2 \tilde{B}_0(m_{\tilde{d}_2}^2, m_{\chi_i^0}^2) \right] \tag{97}
\end{aligned}$$

$$\begin{aligned}
&\quad - \frac{\alpha_W m_d}{12\pi m_W \cos\beta} \tan\theta_W \sum_i N_{i3}^* N_{i1}^* m_{\chi_i^0} \left[ s_d^2 \tilde{B}_0(m_{\tilde{d}_1}^2, m_{\chi_i^0}^2) + c_d^2 \tilde{B}_0(m_{\tilde{d}_2}^2, m_{\chi_i^0}^2) \right], \\
(\Delta m_b)_{\chi^+} &= -\frac{\alpha_W m_t m_b}{8\pi m_W^2 \sin\beta \cos\beta} e^{i\phi_t} c_t s_t (m_{\tilde{t}_1}^2 - m_{\tilde{t}_2}^2) \sum_i U_{i2}^* V_{i2}^* m_{\chi_i^+} I(m_{\tilde{t}_1}^2, m_{\tilde{t}_2}^2, m_{\chi_i^+}^2), \tag{98}
\end{aligned}$$

with

$$\begin{aligned}
I(x, y, z) &= \frac{xy \ln x/y + yz \ln y/z + xz \ln z/x}{(x-y)(y-z)(x-z)}, \\
\tilde{B}_0(x, y) &= \frac{x \ln x - y \ln y}{x-y} \tag{99}
\end{aligned}$$

for the down-type quark, and

$$(\Delta m_e)_{\chi^+} = -\frac{\alpha_W m_e}{4\sqrt{2}\pi m_W \cos\beta} \sum_i U_{i2}^* V_{i1}^* m_{\chi_i^+} \tilde{B}_0(m_{\tilde{\nu}_L}^2, m_{\chi_i^+}^2), \tag{100}$$

$$\begin{aligned}
(\Delta m_e)_{\chi^0} &= \frac{\alpha_W}{4\pi} e^{-i\phi_e} \tan\theta_W s_e c_e (m_{\tilde{e}_1}^2 - m_{\tilde{e}_2}^2) \sum_i N_{i1}^* (N_{i2}^* + \tan\theta_W N_{i1}^*) m_{\chi_i^0} \\
&\quad \times I(m_{\tilde{e}_1}^2, m_{\tilde{e}_2}^2, m_{\chi_i^0}^2) \\
&\quad - \frac{\alpha_W m_e}{8\pi m_W \cos\beta} \sum_i N_{i3}^* (N_{i1}^* \tan\theta_W + N_{i2}^*) m_{\chi_i^0} \left[ c_e^2 \tilde{B}_0(m_{\tilde{e}_1}^2, m_{\chi_i^0}^2) \right. \\
&\quad \left. + s_e^2 \tilde{B}_0(m_{\tilde{e}_2}^2, m_{\chi_i^0}^2) \right] \tag{101} \\
&\quad - \frac{\alpha_W m_e}{4\pi m_W \cos\beta} \tan\theta_W \sum_i N_{i3}^* N_{i1}^* m_{\chi_i^0} \left[ s_e^2 \tilde{B}_0(m_{\tilde{e}_1}^2, m_{\chi_i^0}^2) + c_e^2 \tilde{B}_0(m_{\tilde{e}_2}^2, m_{\chi_i^0}^2) \right]
\end{aligned}$$

for the charged lepton.

The explicit expressions for the contributions to the neutron EDM are given by

$$d_n(d_i, \tilde{d}_q) = 0.7(d_d - 0.25d_u) + 0.55e(\tilde{d}_d + 0.5\tilde{d}_u), \quad (102)$$

$$d_n(w) \sim 20\text{MeV} \times e w, \quad (103)$$

with

$$w(1 \text{ GeV}) = 0.72w(m_b) = -0.72 \times \frac{g_s^3 \tilde{d}_b(m_b)}{32\pi^2 m_b} = -0.68 \times \frac{g_s^3 \tilde{d}_b(M_Z)}{32\pi^2 m_b}, \quad (104)$$

for large  $\tan\beta (\gtrsim 5)$ [12]. Moreover, the four fermion operators contributions to the neutron EDM are estimated as[12]

$$d_n(C_{bd}) \sim \frac{e 0.65 \times 10^{-3} \text{GeV}^2}{m_b} C_{bd}. \quad (105)$$

- 
- [1] A. Pilaftsis and C. E. M. Wagner, Nucl. Phys. **B553**, 3 (1999); M. Carena, J. R. Ellis, A. Pilaftsis, and C. E. M. Wagner, Nucl. Phys. **B586**, 92 (2000).
- [2] S. Y. Choi, M. Drees, and J. S. Lee, Phys. Lett. **B481**, 57 (2000).
- [3] D. A. Demir, Phys. Rev. **D60**, 095007 (1999); S. Y. Choi and J. S. Lee, Phys. Rev. **D61**, 015003 (2000); S. Y. Choi and J. S. Lee, Phys. Rev. **D61**, 115002 (2000); M. Carena, J. R. Ellis, A. Pilaftsis, and C. E. M. Wagner, Phys. Lett. **B495**, 155 (2000); M. Carena, J. R. Ellis, A. Pilaftsis, and C. E. M. Wagner, Nucl. Phys. **B625**, 345 (2002); E. Asakawa, S. Y. Choi, and J. S. Lee, Phys. Rev. **D63**, 015012 (2001); S. Y. Choi, K. Hagiwara, and J. S. Lee, Phys. Rev. **D64**, 032004 (2001); A. G. Akeroyd and A. Arhrib, Phys. Rev. **D64**, 095018 (2001); S. Y. Choi, M. Drees, J. S. Lee, and J. Song, Eur. Phys. J. **C25**, 307 (2002); A. Arhrib, Phys. Rev. **D67**, 015003 (2003); M. Carena, J. R. Ellis, S. Mrenna, A. Pilaftsis, and C. E. M. Wagner, Nucl. Phys. **B659**, 145 (2003); F. Borzumati, J. S. Lee, and W. Y. Song, Phys. Lett. **B595**, 347 (2004); J. R. Ellis, J. S. Lee, and A. Pilaftsis, Phys. Rev. **D70**, 075010 (2004); S. Y. Choi, J. Kalinowski, Y. Liao, and P. M. Zerwas, Eur. Phys. J. **C40**, 555 (2005); S. Y. Choi, K. Hagiwara, and J. S. Lee, Phys. Lett. **B529**, 212 (2002); A. Dedes and S. Moretti, Nucl. Phys. **B576**, 29 (2000); A. Dedes and S. Moretti, Phys. Rev. Lett. **84**, 22 (2000).
- [4] Q.-H. Cao, D. Nomura, K. Tobe, and C. P. Yuan, Phys. Lett. **B632**, 688 (2006).
- [5] P. G. Harris et al., Phys. Rev. Lett. **82**, 904 (1999).

- [6] B. C. Regan, E. D. Commins, C. J. Schmidt, and D. DeMille, Phys. Rev. Lett. **88**, 071805 (2002).
- [7] M. V. Romalis, W. C. Griffith, and E. N. Fortson, Phys. Rev. Lett. **86**, 2505 (2001).
- [8] D. Cho, K. Sangster, and E. A. Hinds, Phys. Rev. Lett. **63**, 2559 (1989); M. A. Rosenberry and T. E. Chupp, Phys. Rev. Lett. **86**, 22 (2001); S. A. Murthy, D. Krause, Jr., Z. L. Li, and L. R. Hunter, Phys. Rev. Lett. **63**, 965 (1989); J. J. Hudson, B. E. Sauer, M. R. Tarbutt, and E. A. Hinds, Phys. Rev. Lett. **89**, 023003 (2002); D. DeMille, F. Bay, S. Bickman, D. Kawall, D. Krause, Jr., S. E. Maxwell, and L. R. Hunter, Phys. Rev. A **61**, 052507 (2000).
- [9] D. Chang, W.-Y. Keung, and A. Pilaftsis, Phys. Rev. Lett. **82**, 900 (1999); D. Chang, W.-F. Chang, and W.-Y. Keung, Phys. Lett. **B478**, 239 (2000).
- [10] K. A. Olive, M. Pospelov, A. Ritz, and Y. Santoso, Phys. Rev. **D72**, 075001 (2005).
- [11] T. Ibrahim and P. Nath, Phys. Rev. **D57**, 478 (1998).
- [12] D. A. Demir, O. Lebedev, K. A. Olive, M. Pospelov, and A. Ritz, Nucl. Phys. **B680**, 339 (2004).
- [13] A. Pilaftsis, Phys. Lett. **B471**, 174 (1999).
- [14] T. Ibrahim and P. Nath, Phys. Rev. **D58**, 111301 (1998).
- [15] A. Dedes and S. Moretti, Eur. Phys. J. **C10**, 515 (1999).
- [16] S. R. Coleman and E. Weinberg, Phys. Rev. **D7**, 1888 (1973).
- [17] D. A. Demir, Phys. Rev. **D60**, 055006 (1999).
- [18] I. J. R. Aitchison (2005), hep-ph/0505105.
- [19] J. R. Ellis, J. S. Lee, and A. Pilaftsis, Phys. Rev. **D72**, 095006 (2005); A. Pilaftsis, Phys. Rev. **D62**, 016007 (2000); T. Falk, K. A. Olive, and M. Srednicki, Phys. Lett. **B354**, 99 (1995); T. Falk and K. A. Olive, Phys. Lett. **B375**, 196 (1996); T. Falk and K. A. Olive, Phys. Lett. **B439**, 71 (1998); T. Ibrahim and P. Nath, Phys. Lett. **B418**, 98 (1998); M. Brhlik, G. J. Good, and G. L. Kane, Phys. Rev. **D59**, 115004 (1999); A. Bartl, T. Gajdosik, W. Porod, P. Stockinger, and H. Stremnitzer, Phys. Rev. **D60**, 073003 (1999); S. Pokorski, J. Rosiek, and C. A. Savoy, Nucl. Phys. **B570**, 81 (2000).
- [20] A. Manohar and H. Georgi, Nucl. Phys. **B234**, 189 (1984).
- [21] I. B. Khriplovich and S. K. Lamoreaux (1997), berlin, Germany: Springer (1997) 230 p.
- [22] M. Pospelov and A. Ritz, Phys. Rev. Lett. **83**, 2526 (1999); D. A. Demir, M. Pospelov, and A. Ritz, Phys. Rev. **D67**, 015007 (2003).

- [23] S. G. Gorishnii, A. L. Kataev, S. A. Larin, and L. R. Surguladze, *Mod. Phys. Lett.* **A5**, 2703 (1990); S. G. Gorishnii, A. L. Kataev, S. A. Larin, and L. R. Surguladze, *Phys. Rev.* **D43**, 1633 (1991); A. Djouadi, M. Spira, and P. M. Zerwas, *Z. Phys.* **C70**, 427 (1996).
- [24] A. Djouadi, J. Kalinowski, and M. Spira, *Comput. Phys. Commun.* **108**, 56 (1998).  
M. Spira, *Fortsch. Phys.* **46**, 203 (1998).
- [25] J. Pumplin et al., *JHEP* **07**, 012 (2002).
- [26] S. Eidelman et al. (Particle Data Group), *Phys. Lett.* **B592**, 1 (2004).
- [27] CDF Collaboration, (2005), hep-ex/0512009.
- [28] C. Kounnas, A. B. Lahanas, D. V. Nanopoulos, and M. Quiros, *Nucl. Phys.* **B236**, 438 (1984);  
J. F. Gunion, H. E. Haber, and M. Sher, *Nucl. Phys.* **B306**, 1 (1988; J. A. Casas, A. Lleyda,  
and C. Munoz, *Nucl. Phys.* **B471**, 3 (1996).

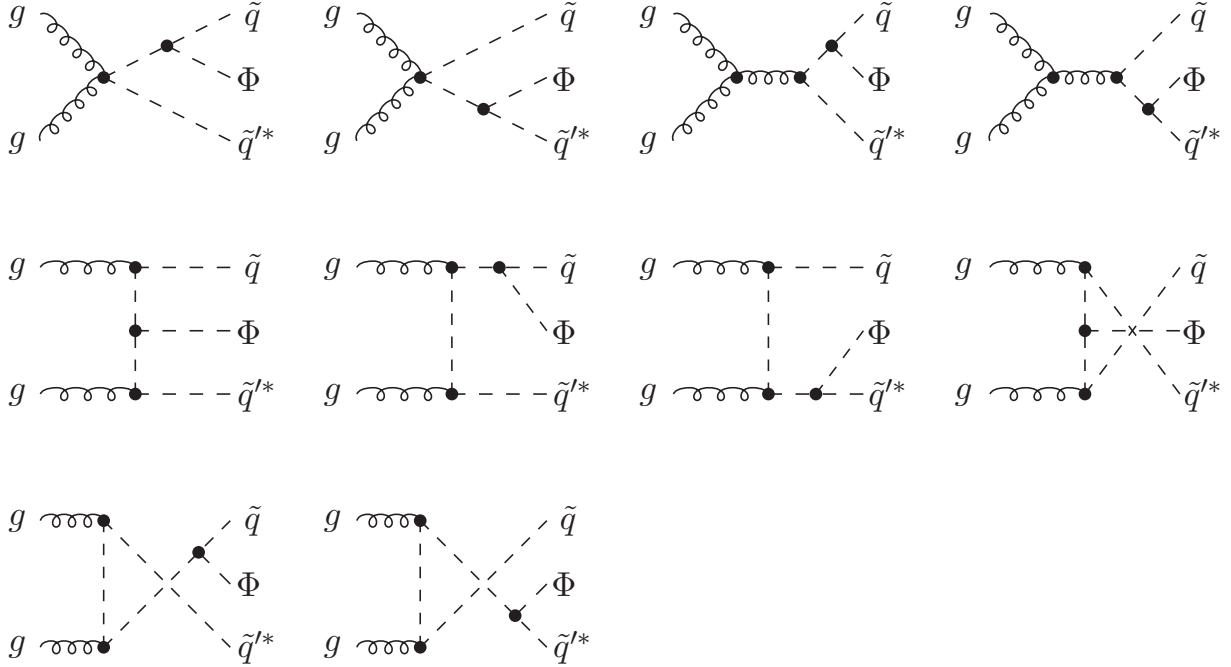


FIG. 1: The Feynman Diagrams for  $gg \rightarrow \tilde{q}_i \tilde{q}_j^* \Phi$ .  $q = t, b$ ,  $i, j = 1, 2$ ,  $\Phi = h_{1,2,3}$  for the CPV and  $\Phi = h^0, H^0, A^0$  for the CPC.

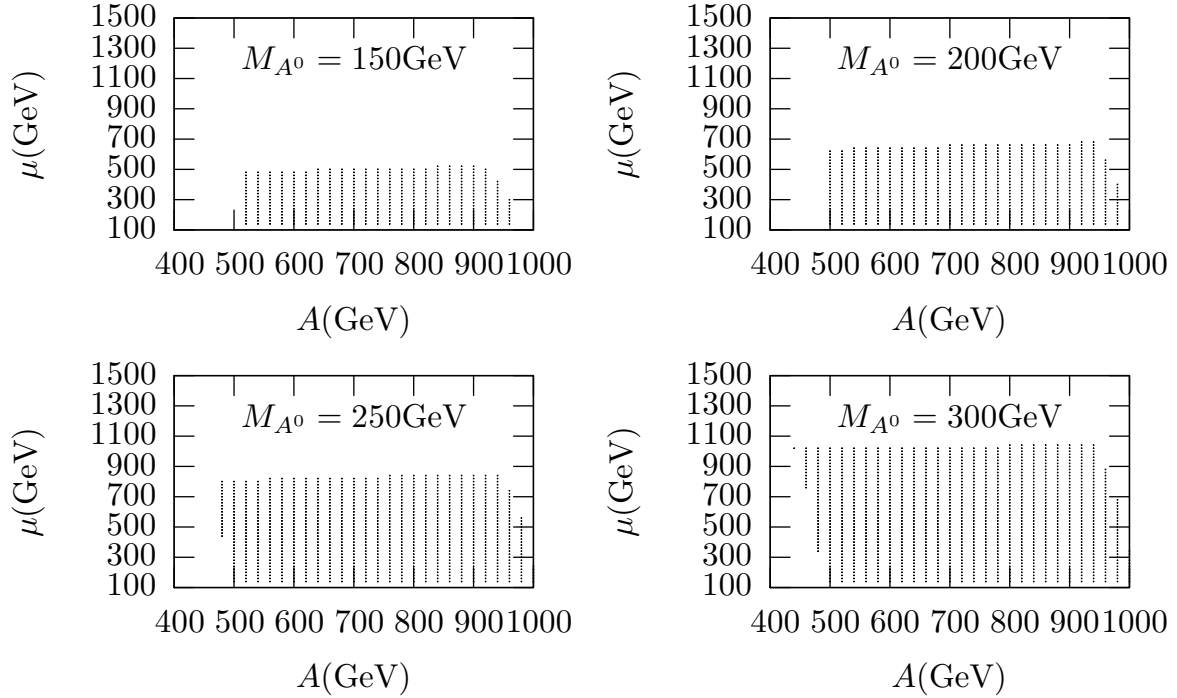


FIG. 2: The allowed ranges of the parameters  $A$  and  $\mu$  for  $\tan\beta = 5$ ,  $m_{\tilde{t}_1} = 100\text{GeV}$ ,  $M_{A^0} = 150\text{GeV}$ ,  $200\text{GeV}$ ,  $250\text{GeV}$  and  $300\text{GeV}$ , respectively.

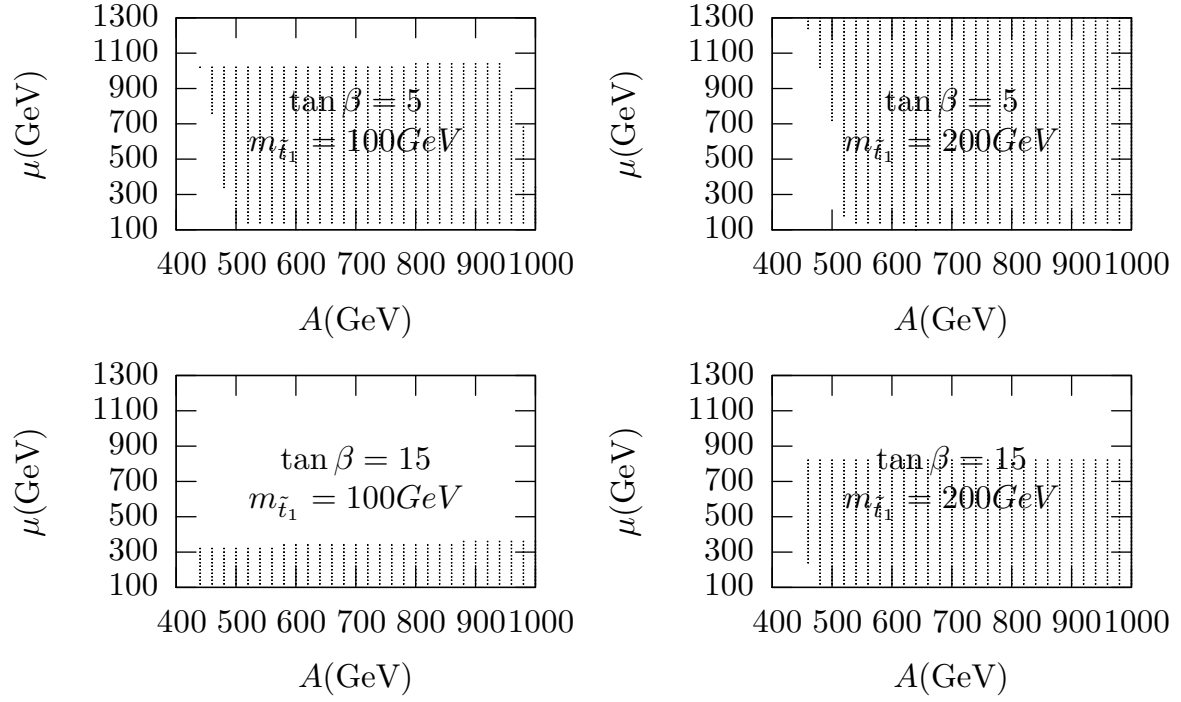


FIG. 3: The allowed ranges of the parameters  $A$  and  $\mu$  for  $M_{A^0} = 300 \text{ GeV}$ ,  $\tan \beta = 5$  and  $15$ ,  $m_{\tilde{t}_1} = 100 \text{ GeV}$  and  $200 \text{ GeV}$ , respectively.

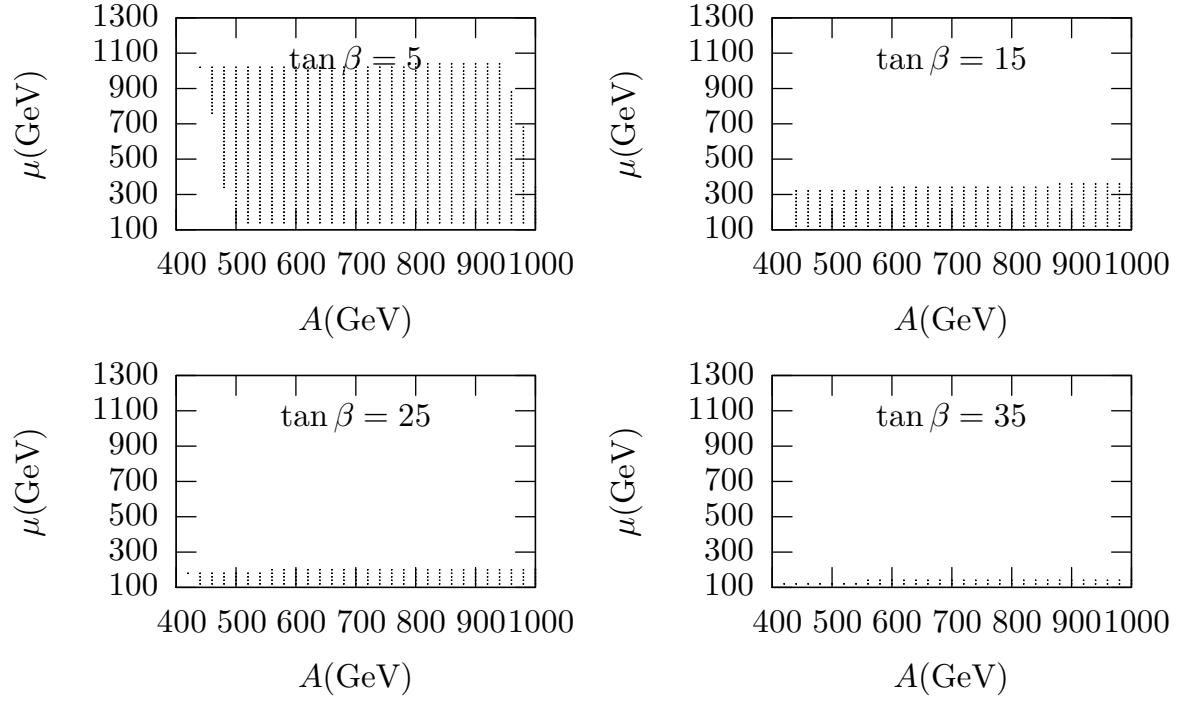


FIG. 4: The allowed ranges of the parameters  $A$  and  $\mu$  for  $M_{A^0} = 300\text{GeV}$ ,  $m_{\tilde{t}_1} = 100\text{GeV}$ ,  $\tan \beta = 5, 15, 25$  and  $35$ , respectively.

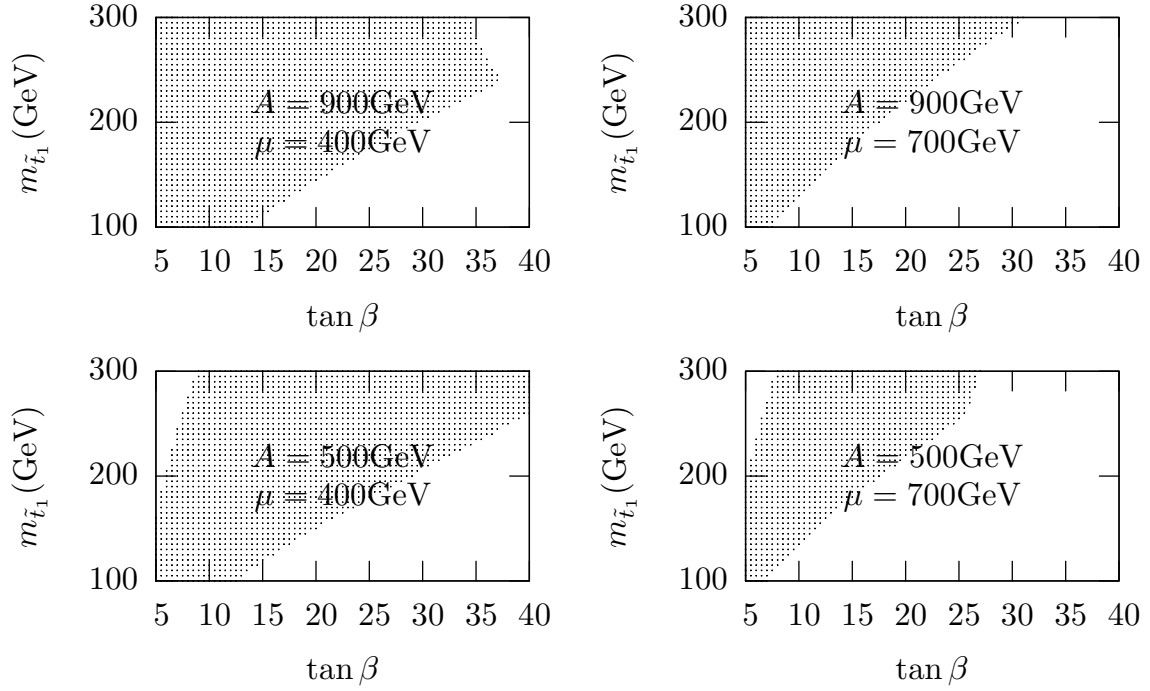


FIG. 5: The allowed ranges of the parameters  $\tan \beta$  and  $m_{\tilde{t}_1}$  for  $M_{A^0} = 300\text{GeV}$ ,  $A = 500\text{GeV}$  and  $900\text{GeV}$ ,  $\mu = 400\text{GeV}$  and  $700\text{GeV}$ , respectively.

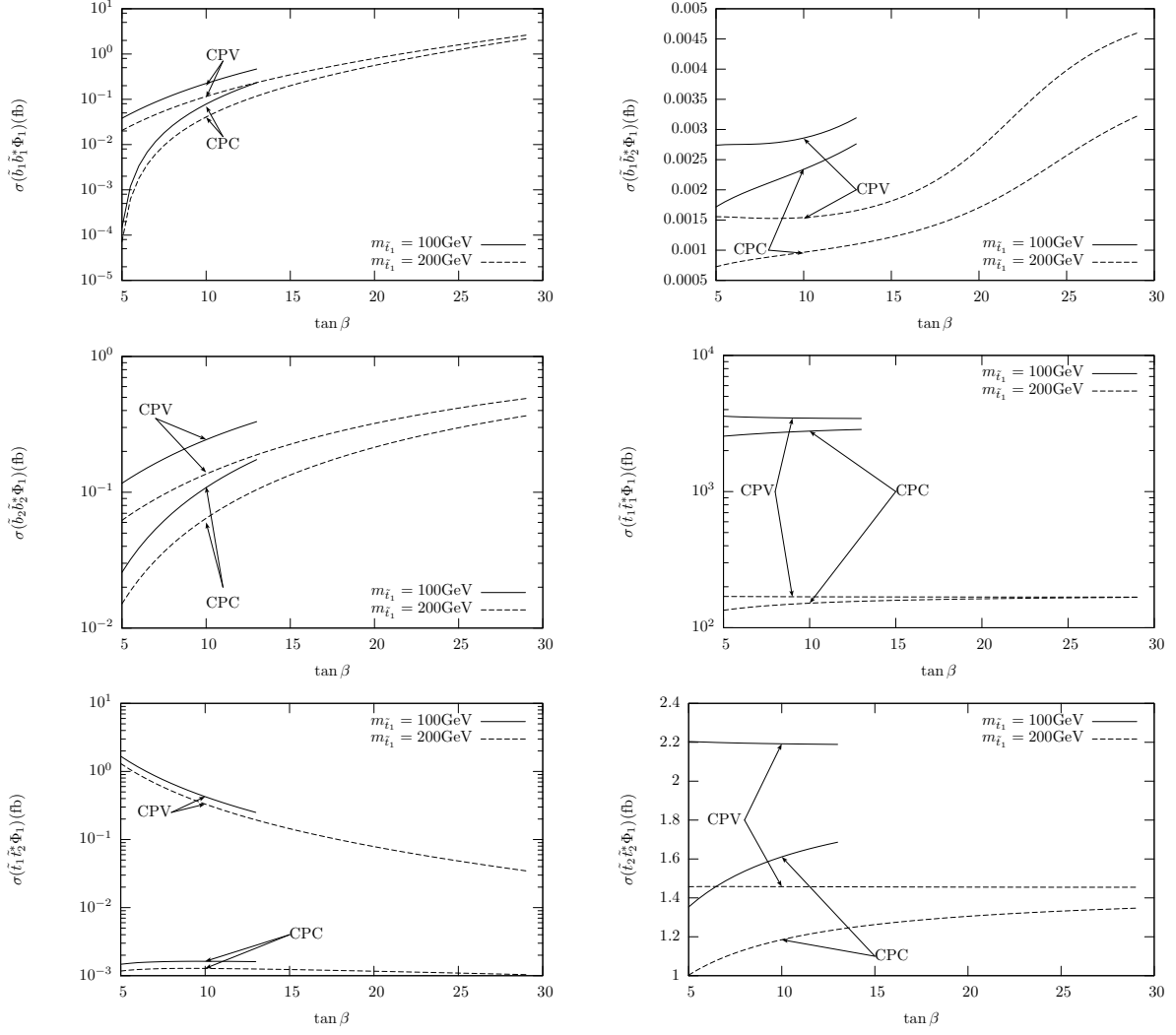


FIG. 6: The cross sections of  $\Phi_1$  productions associated with squark pairs as the functions of  $\tan \beta$ , where  $\Phi_1 = h^0$  in CPC and  $\Phi_1 = h_1$  in CPV.  $A = 900$  GeV and  $\mu = 400$  GeV.

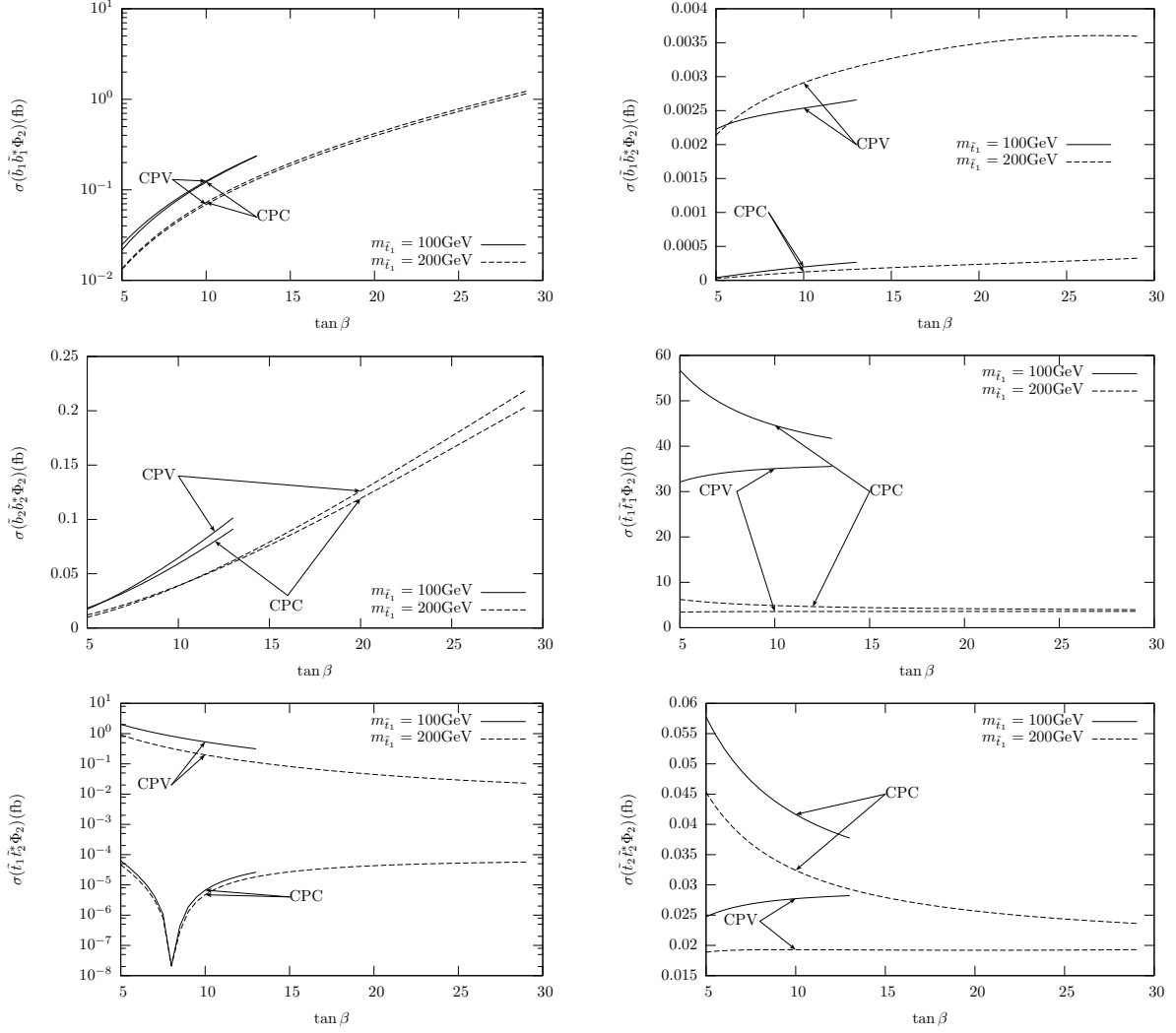


FIG. 7: The cross sections of  $\Phi_2$  productions associated with squark pairs as the functions of  $\tan \beta$ , where  $\Phi_2 = H^0$  in CPC and  $\Phi_2 = h_2$  in CPV.  $A = 900$  GeV and  $\mu = 400$  GeV.

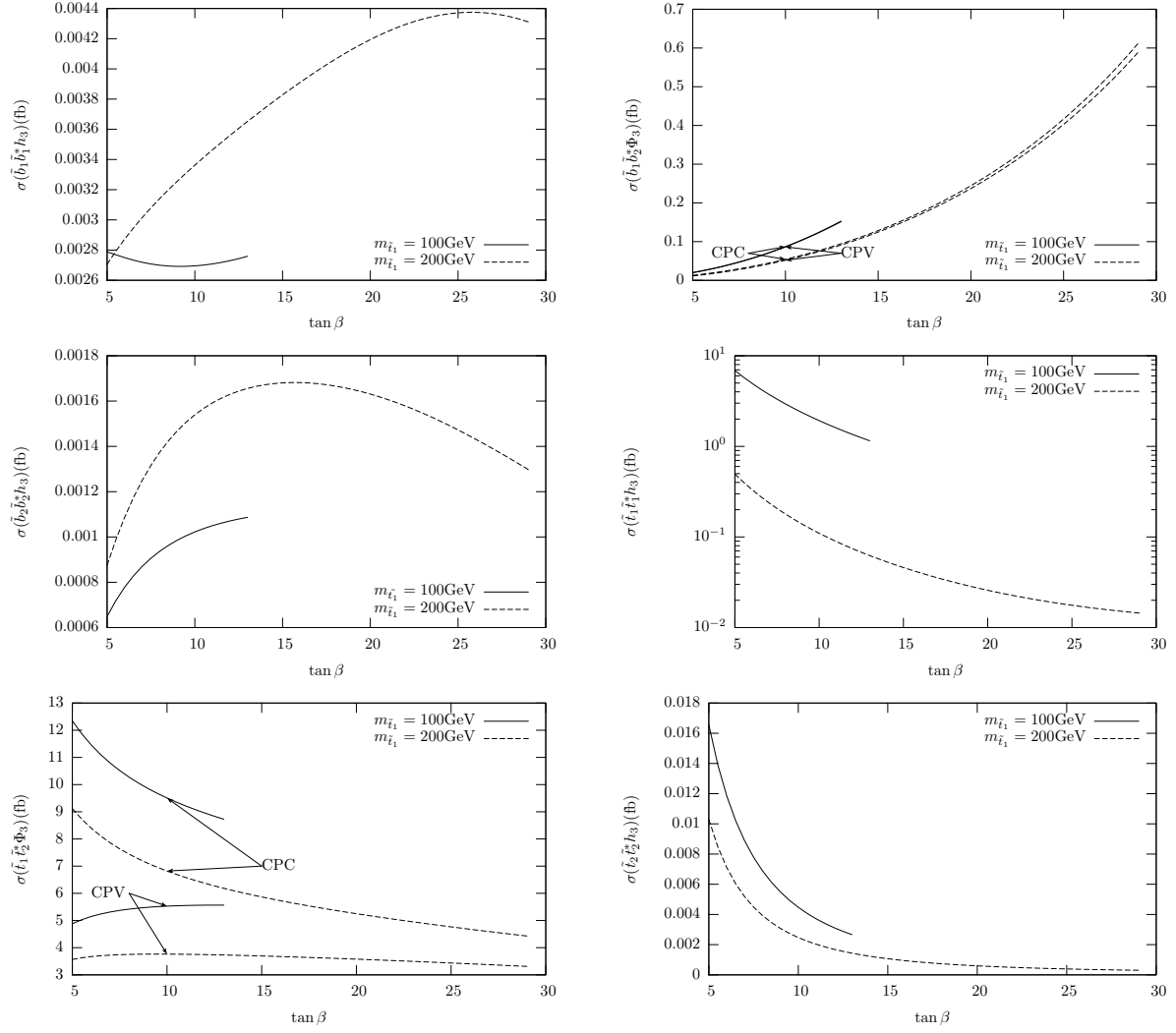


FIG. 8: The cross sections of  $\Phi_3$  productions associated with squark pairs as the functions of  $\tan \beta$ , where  $\Phi_3 = A^0$  in CPC and  $\Phi_3 = h_3$  in CPV.  $A = 900$  GeV and  $\mu = 400$  GeV.

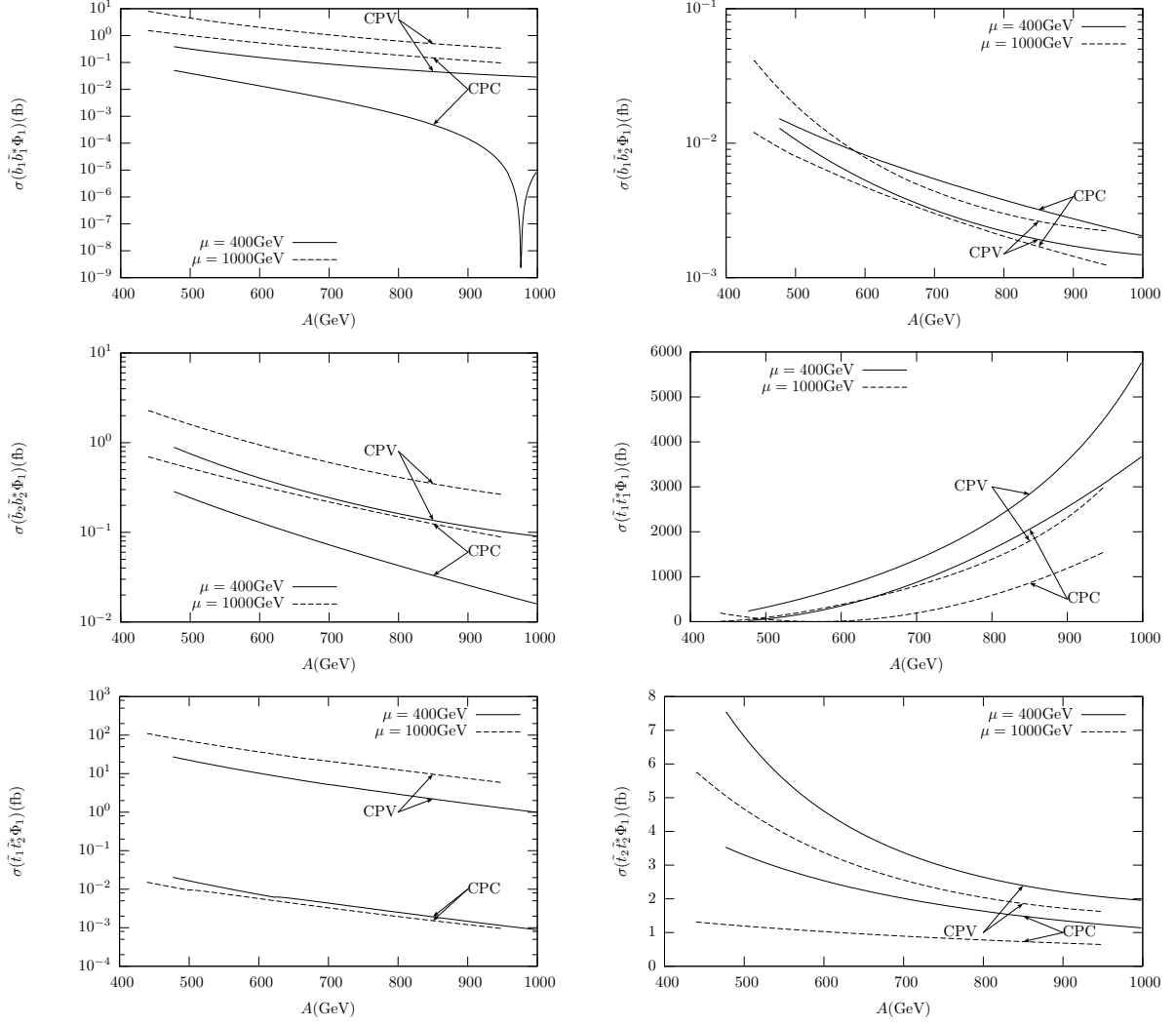


FIG. 9: The cross sections of  $\Phi_1$  productions associated with squark pairs as the functions of  $A$ , where  $\Phi_1 = h^0$  in CPC and  $\Phi_1 = h_1$  in CPV.  $\tan\beta = 5$  and  $m_{\tilde{t}_1} = 100$  GeV.

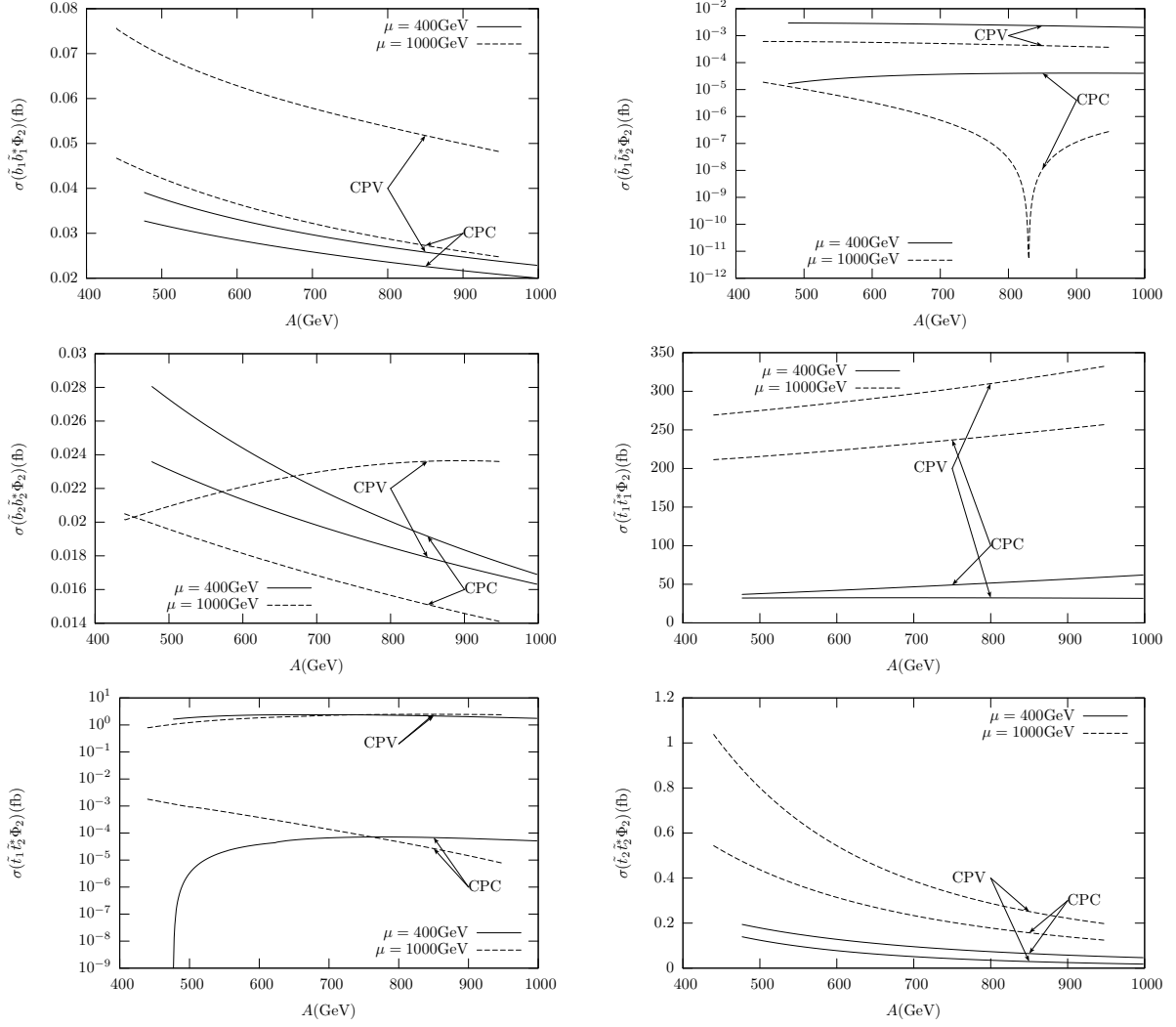


FIG. 10: The cross sections of  $\Phi_2$  productions associated with squark pairs as the functions of  $A$ , where  $\Phi_2 = H^0$  in CPC and  $\Phi_2 = h_2$  in CPV.  $\tan\beta = 5$  and  $m_{\tilde{t}_1} = 100$  GeV.

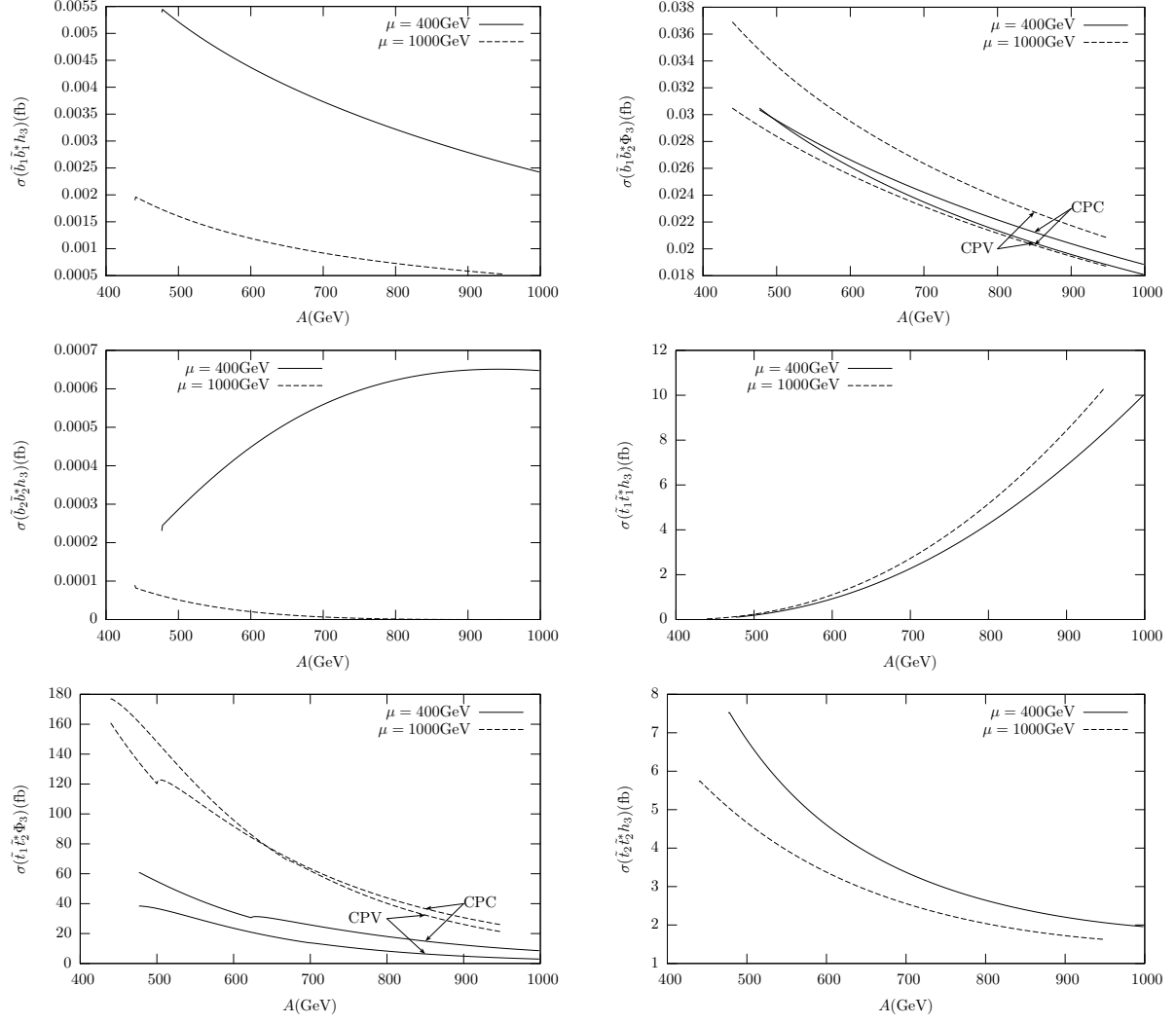


FIG. 11: The cross sections of  $\Phi_3$  productions associated with squark pairs as the functions of  $A$ , where  $\Phi_3 = A^0$  in CPC and  $\Phi_3 = h_3$  in CPV.  $\tan \beta = 5$  and  $m_{\tilde{t}_1} = 100$  GeV.